Photoluminescence and optical properties of glass and glass-ceramics derived from hybrid sources

A Thesis submitted in partial fulfillment of the requirements for the Degree of

MASTER OF SCIENCE

in

PHYSICS

Submitted by

ANSHU GARG

Roll No. 302204002

Under the Guidance of

Dr. Kulvir Singh

Head and Professor, DPMS

2024

Department Of Physics and Material Science

Thapar Institute of Engineering & Technology, Patiala

(Declared as Deemed-to-be-University u/s 3 of the UGC Act., 1956)

Post Bag No. 32, Patiala – 147004

Punjab (India)

DECLARATION

I hereby certify that the work which is presented in the dissertation entitled, "**Photoluminescence and optical properties of glass and glass-ceramics derived from hybrid sources**", in partial fulfillment of the requirements for the award of the degree of Masters In Physics, Department of Physics and Material Science, Thapar Institute of Engineering & Technology (Deemed to be University) is an authentic record of my work carried under the supervision of Dr. Kulvir Singh. It refers to other researcher's work duly listed in the reference section. The matter in this dissertation has not been submitted, neither in part nor in full to any other degree to any other university or institute except as reported in text and references.

(Anshu Garg)

Date: 31st July 2024 **Roll No.: 302204002**

It is certified that the above statement made by the student is correct to the best of my knowledge and belief.

(Dr. Kulvir Singh)

Date**:**31st July 2024 **Head & Professor**

Department of Physics and Material Science,

Thapar Institute of Engineering &Technology, Patiala

CERTIFICATE

I hereby certify that the dissertation entitled **"Photoluminescence and optical properties of glass and glass-ceramics derived from hybrid sources"** is an authentic record of my work carried out for partial fulfillment of the requirements for the award of M.Sc. Physics, to Thapar Institute of Engineering & Technology (Deemed to be a university), is under the guidance of **Dr. Kulvir Singh,** HOD and professor, Department of Physics and Materials Science. The matter of this report has not been submitted in part or full to any university or institute for the award of any degree.

(Dr. Kulvir Singh)

Date: 31st July 2024

Supervisor

ACKNOWLEDGMENT

First of all, I would like to thank the “Waheguru”, for his mercy and blessing to me, which helped me to complete my work.

I would like to thank several people who have provided tremendous support and always encouraged me to complete my thesis work. I like to express my sincere gratitude to my supervisor Dr. Kulvir Singh for his unlimited guidance, motivation, and above all his ever-co-operating attitude toward me in bringing up this thesis in its present elegant form. His meticulous attention to my proceedings, his devoted time, and his ideas have enabled me to make the project a success. My special thanks to all the Department of Physics and Materials Science faculty who have always been helpful to me throughout my work.

I am indebted to Ms. Navneet Kaur for her unconditional support and motivation in completing my research work. I am grateful to my all friends for their constant support and encouragement to complete my work.

Last but not least, my heartiest thanks to my parents for their moral support and love, without their support it was not possible to come so far.

Anshu Garg

(302204002)

Abstract:

The composition $43SiO_2$-$25CaO$-$25Na_2O$-$7P_2O_5$ (%wt) was synthesized using SiO_2 and CaO driven from agro-food waste and conventional chemicals using the melt quench technique. The glass sample was further doped with different rare-earth ions i.e., Dy^{3+}, Eu^{3+}, Sm^{3+}, and Pr^{3+} followed by heat treatment to convert glass into glass-ceramics. Further, the heat-treated samples are characterized using various characterization techniques such as x-ray diffraction (XRD), Fourier Transform infra-red spectroscopy (FTIR), Raman spectroscopy, UV-visible spectroscopy (Uv-vis), photoluminescence spectroscopy to check their applicability as phosphor materials for LED applications. XRD indicates the formation of sodium-calcium silicate phase in all the samples. The optical band gap falls in the range of 3.76-3.60 eV. The CIE coordinates indicate the present samples fall in different color regions and can be used as suitable phosphor materials.

TABLE OF CONTENTS

LIST OF FIGURES

LIST OF TABLES

1. Glasses

Glass is an amorphous material that remains unnoticed despite its great usage. It is so common that we often forget to acknowledge it. Glass is everywhere, from our mobile screens or watches to windows of multistorey buildings. But how do we define glass. Glass is a transparent material that lacks long-range order, and periodic arrangement and exhibits glass transition behavior. Any material, inorganic, organic, or metallic that showcases glass transition behavior can be called glass [1].

1.1. Characteristics of glass

Glass transition behavior is not observed at a particular temperature but over a particular range. The temperature range over which glass transformation behavior is observed is known as glass transformation or transition temperature (T_g). It is defined as the range over which an amorphous material undergoes a transition from a hard and brittle solid to a rubbery and highly viscous state with an increase in temperature. Below T_g, the material behaves as solid having a rigid structure but as we move towards T_g properties change. After T_g, the material behaves as a viscous liquid having more freedom of movement [1]. It can be better understood from the enthalpy temperature diagram.

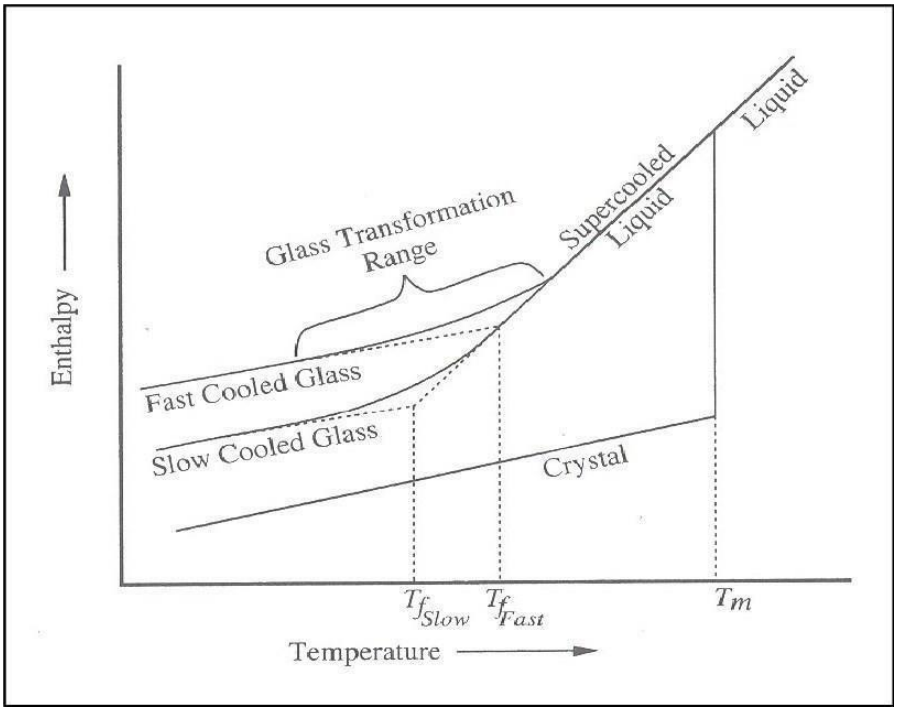

Fig. 1.1. Enthalpy temperature diagram for glass and crystal [1]

If the cooling rate of liquid is appropriate, then below melting point crystallization is observed and a sudden drop in enthalpy is visible. If the cooling rate is fast then a supercooled liquid is obtained

which avoids crystal nucleation and growth. As the temperature decreases further, an increase in viscosity is observed. At some point, the increase in viscosity is enough to put an end to the rearrangement of atoms to get liquid structure. Soon the enthalpy deviates from the equilibrium line and reaches a frozen liquid state. This frozen liquid is glass [1].

1.2. Structure of glass

During the initial stage, every observed glass was generally a silicate glass so it was assumed that only silicates possess the properties to be transformed into glass. But in recent years many non-silicate glasses have been observed which leads to the failure of this assumption. Old theories focused on the structure of glass and many theories came up with the idea to explain the structure of glass formation.

Among these Zachariasen's theory is widely accepted. It provided a framework for understanding the formation of glasses and the arrangement within it. He noticed that silicates that form glasses rapidly do not have crystalline structures and do not have periodic or symmetric arrangements, which might be the final condition for the formation of glass. To better understand the structure of glasses, he gave a set of rules [1]:

1. Every oxygen atom can be linked to a maximum of two cations.
2. Oxygen polyhedra can share only corners and not edges or faces.
3. The coordination number of oxygen of network cation should be small.
4. At least 3 corners of oxygen polyhedron are to be shared to form a 3-dimensional structure.

1.3. Components of glass

Glass composition consists of various ions from the periodic table present in different amounts. Based on their percentage these ions play different roles in the glass matrix. Based on their role materials are classified into five categories:

i. Network formers
ii. Glass intermediates
iii. Glass modifiers
iv. Colorants
v. Fining Agents

1.3.1. Network formers

These cations are the most important components of glass as they can form strong covalent bonds. They have high electronegativities and form good glasses. These include network cations such as

SiO_2, B_2O_3, P_2O_5, etc [2]. Glass formers have high field strength $F \geq 1.5$ $Å^{-2}$ as compared to modifiers and intermediates [3]. These contribute to the mechanical strength and hardness of glasses [1].

1.3.2. Network modifiers

The group of cations that have very low electronegativity, and cannot form glasses on their own is known as glass modifiers. They form highly as compared to formers and intermediates and have low field strength $F \leq 0.4$ $Å^{-2}$ [3]. These cations interact with network formers modify the glass network and change its properties. The MgO, CaO, Na_2O, K_2O, etc. [2] are mostly used as glass modifiers in the glass network structure.

1.3.3. Intermediates

As the name suggests intermediates are the ones that lie in between network formers and modifiers. Their role keeps on changing as network formers or modifiers depending on their percentage in the matrix. Intermediates do not form glass networks of their own but can replace the formers, which results in the changed properties of the glasses. The field strength of these intermediates lies in between formers and modifiers i.e., $0.5 \leq F \leq 1.0$ $Å^{-2}$ [3]. This type of behavior of intermediates is attributed to their various coordination states. The most common intermediates are Al_2O_3, ZrO_2, etc.

1.3.4. Colorants

Colorants are used to impart color to the glass. The majority of colorants include either 3d transition metals oxides or 4f rare earth elements. Copper, nickel, gold, and silver are used as colorants. The intensity and shade of color depend upon the type and amount of colorant used [1].

1.3.5. Fining agents

These are used for the removal of bubbles and to increase the quality of glass. Fining agents include NaCl, NaF, potassium and sodium nitrates, and several sulfates. Generally, very small quantities of these materials are used.

1.4. Properties of glass

Glass is a unique material with a liquid-like structure that gives rise to its special properties. Some of these properties are explained below**:**

1.4.1. Physical: Glasses are transparent which allows visible light to pass through them. The density of glass depends upon its composition. Density is considerably modified by crystallization. Glasses can also be permanently compacted by application of very high pressures.

1.4.2. Mechanical: Glasses are brittle materials and when stress is applied, they exhibit nearly perfect Hookian behavior. Fracture strength is less than the theoretical strength and is controlled by the environment and the concentration of flaws present on the surface. The strength of glasses usually decreases with time under normal conditions. Thermal shocks lead to glass cracking and failure [4]. Thus, glasses should be handled with care to maintain their strength.

1.4.3. Thermal: Vitreous silica and a few other fully linked glass networks showcase negative thermal expansion coefficients. Glasses are very useful for applications where insulating material having a low coefficient of thermal expansion is required.

1.4.4. Electrical: The composition of glass has a vital role in the electric conductivity of glasses. Generally, the glasses are insulating in nature. These types of glasses are free from any network modifiers. The electrical conductivity of glasses is altered by the introduction of modifiers in the matrix due to the mobility of alkali or oxide ions [5,6].

1.4.5. Optical: Glasses find numerous applications in the field of optics. These applications are based on various optical properties such as transmission, absorption, reflection, scattering, and refractive index. These properties are mainly altered by glass compositions rather than the melting process and thermal treatment [7].

1.5. Glass ceramics

Glass-ceramics are materials in which crystalline phases are embedded in the glass matrix obtained by the controlled crystallization of glasses [8]. Glass-ceramics are known for their unusual combination of properties. Controlled nucleation and crystallization of glass leads to the formation of glass-ceramics. Initially, the glasses are melted and shaped and then after heat treatment, they are converted into crystalline ceramics. Glass-ceramics were invented by famous glass chemist Dr. S.D. Stookey in the mid-1950s [9].

Stookey [10] invented an almost fully crystallized glass in composition Li_2O-Al_2O_3-SiO_2 or MgO-Al_2O_3-SiO_2 systems containing 2-20 wt% TiO_2. The glass after crystallization showed extreme change in thermal expansion and mechanical strength though they maintained the original glass article shape [11]. The method of forming glass-ceramic by glass devitrification is a heterogeneous transformation. It consists of two stages i.e. nucleation stage and growth stage [12].

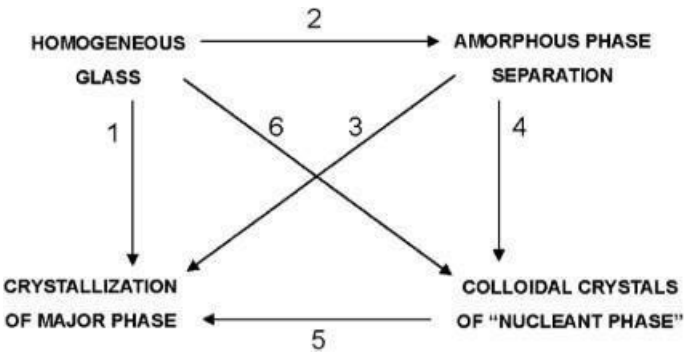

Fig. 1.2. Reaction paths between the initial glass and final glass-ceramic [11]

All glasses can't be converted into ceramics. Some glasses are too stable and difficult to crystallize whereas some crystallize uncontrollably [13]. The glass composition also plays an important role here. Glasses include metals, polymers, and inorganic and organic materials while on the other hand, the term glass-ceramics is only used for inorganic and non-metallic materials [14]. Glass-ceramics are not completely crystalline; mostly the microstructure is 50-95 vol% crystalline [15]. Glass- ceramics offer a diverse array of physical and chemical properties that are difficult to achieve in parent glass. However, the process of fabrication of glass-ceramics has its limitations. The properties of glass-ceramics depend largely on the parent glass composition.

Glass-ceramics are categorized into two subgroups: oxide and non-oxide. Oxide glass-ceramics include borate (B_2O_3), silicate (SiO_2), and phosphate (P_2O_5) type materials. Non-oxide glass-ceramics include halide, chalcogenide, and metallic types [16]. Nowadays focus has extremely shifted to the applications of glass-ceramics due to their better properties. Their use has expanded into major four categories i.e. electronics, medicine and dentistry, optical materials, and thermal-mechanical environments. Out of their various optical applications, some include luminescent glass-ceramics for solar concentrators, up-conversion, and amplification devices; heat-resistant materials that absorb UV, reflect IR, and are transparent to visible light; materials that absorb UV and fluoresce in red/IR; substrates for arrayed waveguide grating; and laser pumps [13]. They even serve as good hosts for transition metal ions [17].

The major drawback of glass-ceramics over single crystal is that dopants are not necessarily located in the desired phase but dispersed between different amorphous and crystalline phases and at their interfaces, which adds to the optical losses of the material [16].

1.6. Agro-food waste as a resource for glass

The fact that waste levels are increasing day by day is known to everyone, and its negative impacts are also not a hidden factor. With a growing population, the most basic requirement of food faces a tremendous increase in demand. The pressure to meet this increase in market demand leads to overproduction of crops. Inefficient harvesting techniques, inadequate infrastructure, poor storage facilities, bad transportation, and many other factors lead to the wastage of food. Thus, it is referred to as agro-food waste. This waste includes a broad range of fruits, crops, grains, dairy products, meats, leaves, husks, etc [18,19]. According to the latest statistics, approximately one-third of all the food produced is lost annually, amounting to about 1.3 billion metric tons of food waste annually. Food waste is lower in developing countries as compared to developed countries. The US is one of the largest contributors to food waste globally, amounting to about 60.3 million metric tons of food waste annually.

Traditionally, this waste was used as fertilizer as it is biodegradable, which required a lot of time and patience but in today's fast-paced world, no one wants to wait and demands instant results. So, this method is not very popular these days.

Biomass being a renewable source is utilized to synthesize various value-added materials. This waste also serves as a fuel source in place of fossil fuels (oil, natural gas, and coal) [20]. For this purpose, the waste is burnt in the air leading to air pollution and emission of greenhouse gases such as carbon dioxides, carbon monoxide, oxides of sulfur, and nitrogen. These greenhouse gases cause ozone layer depletion, glacier melting, acid rain, forest fires, and many more environment-related issues. Lack of effective and safe ways to manage these wastes leads to a direct impact on human health [21]. One more issue related to this is that they leave behind ashes. These ashes are considered as the second-generation byproducts. These ashes contain different useful elements in oxide form which is why they find applications in many fields [22].

To study their applications, it is a must to have a complete knowledge of their physical and chemical properties. The content of various metal and metalloid oxides depends upon the region, quality of soil, fertilizers used during their growth, and burning atmosphere. Cornejo et al. [23] reported the chemical compositions of various agro-food wastes. RHA and ES contain high levels of SiO_2 and CaO respectively. SCLA, WSA, and other agricultural waste ashes contain some trace elements like K_2O, Na_2O, and MgO besides 30-78% SiO_2 with 22% carbon content [24]. Based on their different compositions these ashes find applications in various fields like glass and glass-ceramics, cement and civil construction, bioactive materials and bioglasses, and silicate-based ceramics directly or

indirectly. According to some recent reports that have appeared in the literature some properly selected agro-food waste ashes can be used to produce glasses, and glass-ceramics [23,25].

1.7. Optical properties of agro-food waste-derived glass

Recently, ashes from agro-food waste have been utilized to create glasses and glass-ceramics for windows, optical devices, and other uses [26]. Calcium silicate phosphor hosts are generally synthesized from mineral oxides but it is preferable to use readily accessible agro-food wastes as sources of SiO_2 and CaO. This strategy is favorable as it offers a low-cost biomass waste management technique without resulting in air pollution. All the existing waste ashes have a major content of silica, which can be used as an alternative to commercially available silica. The main intention of this study is the development of phosphors with better luminescence properties by using agro-food waste materials [25]. Besides this, these glasses contain small amounts of transition metal oxides inherently which make them advantageous over conventional glasses. Therefore, in glasses and glass ceramics generated from agro-food waste, the existence of these fundamental trace element oxides serves as active centres for photoluminescence. Cornejo et al. [23] reported that from RHA and ESP along with a small amount of NaCl and alumina, a window glass can be synthesized. It is a known fact that the silicate matrix has the ability to serve as a suitable host for producing phosphors. Punj et al. [25] used CHA, SCLA, and ESP to synthesize silicate-phosphor glasses. These glasses emit blue-green light because naturally occurring trace element oxides i.e. TiO_4 are present in them. Rare-earth ions can act as efficient luminescent centers due to their special 4f configuration. Devi et al. [27,28] synthesized monoclinic Ca_2SiO_4 using eggshells and rice husk ash which were further doped with Eu^{3+} and Dy^{3+}. The photoluminescence data revealed the emission of red and white light, respectively, hence, they find applications in producing LEDs.

Chapter 2 Literature Review.

This chapter aims to present the work done so far in the study of silicate glasses and glass-ceramics as phosphors, and the effect of the addition of rare earth ions for the photoluminescent applications.

Zhu et al. [29] conducted a study on rare earth Ce^{3+}, Tb^{3+}, and Eu^{3+} doped silicate and phosphate glasses. These glasses were synthesized using the melt-quenching technique. A combination of blue, green, and red bands was observed in both glasses. When the glass was excited by UV light it emitted white light. The glass samples exhibited tunable emissions in the green, blue, and red regions. For silicate glasses, by varying the concentration of Eu^{3+} ions a change in the intensity ratio of red to green emissions is observed. Eu3+ and Ce3+ ions contributed to the emission intensity ratio in phosphor glasses. This made it more effective for developing white LEDs.

Caldino et al. [30] studied the effect of rare earth-doped glasses on displays and light generation. They studied zinc sodium aluminosilicate glasses that were doped with various rare earth elements. These glasses were singly doped with Eu^{3+}, $Tb^{3+,}$ or Sm^{3+} and co-doped with combinations like Tb^{3+}-Eu^{3+}, Tb^{3+}-$Sm^{3+,}$ and Tb^{3+}-Ce^{3+}. The glass matrix composition was $60SiO_2$-$18Na_2O$-$12K_2O$-$5ZnO$-$5Al_2O_3$. The ability to control the emission band allowed the usage of glasses in LEDs, optical amplification, frequency conversion, and integrated optical devices.

Kesavulu et al. [31] synthesized gadolinium calcium silica borate glasses doped with Er^{3+} having composition (55-x) B_2O_3-$10SiO_2$-25 Gd_2O_3-10 CaO-x Er_2O_3, where x = 0.0, 0.5, 1.0, 1.5, 2.0 and 2.5 mol % using melt quenching method. They observed the decrease in indirect band gap energy with an increase in erbium ion concentration, due to the formation of a greater number of non-bridging oxygens (NBOs). They reported that these glasses hold great potential as hosts for the advancement of lasers and broad-band optical amplifiers.

Devi et al. [27] synthesized a series of Ca_2SiO_4 phosphors doped with Dy^{3+} ions using solid-state reaction method. Raw materials were extracted from the agricultural waste of rice husks and eggshells. XRD patterns confirmed that the phosphors are crystallized in a monoclinic structure. The emission spectra revealed that the color coordinates fall within the white light zone. The change in fluorescence decay curves was observed due to dipole-dipole interactions of Dy^{3+} ions. Their suitability for inexpensive white light-producing devices was verified by these results.

Niu et al. [32] synthesized oxyfluoride silicate glasses doped with Pr^{3+} by melt quenching technique. The raw materials used were SiO_2, Al_2O_3, H_3BO_3, ZnO, CaF_2, $CaCO_3$, Na_2CO_3 and high purity Pr_2O_3. When Al_2O_3 and ZnO were incorporated into the sample they promoted $^3P_0 \rightarrow {}^3H_4$ emission transition

of Pr^{3+} ions. Self-excitation of Pr^{3+} ions was observed at 443 nm. These results proved that the rare earth-doped glasses could be used to develop lighting devices.

Devi et al. [33] synthesized phosphors of $Ca_2SiO_4:xSm^{3+}$ (x=0.1,02,0.3,0.05 and 0.01 mol%) through SSR technique at 1250^{o}C for 8 h. Here SiO_2 and CaO were extracted from rice husk and egg shells respectively. XRD patterns confirmed that the crystal is monoclinic and matches with ICDD card No. 01-076-3612. CIE color coordinates represented the reddish-orange emission of the Sm^{3+} ions. As the concentration of Sm^{3+} ions were increased in the sample, its lifetime decreased. These results concluded that $Ca_2SiO_4:xSm^{3+}$ phosphors have the potential to be used in the manufacture of low-cost white light-emitting diodes.

Niu et al. [34] conducted a study on Eu and Dy doped borophosphosilicate glass-ceramics which were prepared by melt quenching method followed by heat treatment, using pure reagents such as SiO_2, H_3BO_3, NH_4HPO_4, Al_2O_3, Na_2CO_3, and high purity rare earth oxides Eu_2O_3 and Dy_2O_3 as raw materials. X-ray patterns showed the formation of $AlPO_4$ crystals in the glass matrix occurred leading to the formation of glass-ceramics. The relative content of B_2O_3 and P_2O_5 influenced the glass-ceramics' structure. By adjusting the B_2O_3/P_2O_5 content and the doping level of Eu ions the emission color of glass-ceramics was effectively controlled. These glass-ceramics became promising applicators in light-emitting diodes.

Rodriguez et al. [35] synthesized a glass matrix having a chemical composition of $55SiO_2$-27SrO-18MgO (mol%) doped with Sm_2O_3 and co-doped with Sm_2O_3/Dy_2O_3 using the melt-quenching technique. When doped with rare earth metals, these glasses transform into glass-ceramics after sintering and crystallization. XRD patterns revealed the formation of the Sr-akermanite $Sr_2MgSi_2O_7$ phase. In excitation and emission spectra different peaks for Sm^{3+} and Dy^{3+} ions were observed indicating that there is no energy transfer between these ions. With a change in excitation wavelength CIE coordinates also changed indicating that these glasses can emit different colors based on the excitation wavelength and can be used in photonic devices operating in visible regions.

Gao et al. [36] developed a glass with a composition in mol% $40SiO_2$-$25Al_2O_3$-$15Na_2CO_3$-$10YF_3$-10NaF-$1EuF_3$-xAl (x=1, 3, 6, and 10). After heat treatment at 620^{o}C peaks were observed in XRD patterns corresponding to the $NaYF_4$ phase. The ratio of Eu^{3+} to Eu^{2+} changed when glass-ceramics were subjected to heat treatment. With an increase in Al concentration, the chromaticity coordinates moved from the red-light region to the white light region and blue light region indicating their potential to be used as luminescence sources in LEDs due to their ability to emit different colors i.e. red, white, and blue.

Li et al. [37] synthesized a base glass with a molar ratio of $48B_2O_3$–$27CaF_2$–$18Bi_2O_3$–$3ZnO$–$4Al_2O_3$ and then doped it with 1 mol% of Yb_2O_3 and 0.5 mol% Er_2O_3. Through techniques like XRD, TEM, and HRTEM the presence of CaF_2 crystallites within the glass matrix was confirmed. The temperature at which heat treatment was employed affected the number of crystal particles which in turn affects light transmittance. CaF_2 nanocrystals provided a favorable luminescence environment for Er^{3+} ions. Chinna et al. [38] conducted a study to synthesize Ca_2SiO_4:Eu^{3+} phosphors using agro-food waste and further use it for LED applications. These phosphors were synthesized from rice husk ash and eggshell powder via a solid-state reaction method. They had varying Eu^{2+} concentrations (0.25%,0.50%,0.75% and 1.00%). The presence of the Ca_2SiO_4 phase was validated by XRD patterns. The value of the optical band gap (Eg) was observed in the range 3.62–3.79 eV. The CIE coordinates of Eu^{3+}, Eu^{2+}, and Ti^{4+}, activated Ca_2SiO_4 lie in the green region. The optical characteristics of these waste-derived phosphors determined that they could be employed for solid-state lighting applications.

Monisha et al. [39] synthesized glass matrix $20SiO_2$-$19.5B_2O_3$-$10Al_2O_3$-$10ZnO$-$30NaF_2$-$10ZnFe$-$0.5Sm_2O_3$ with 0.5 mol% Sm^{3+} doping by melt quenching process followed by heat treatment at 500^{o}C for 3 h. XRD patterns confirmed the presence of the $Sm_2Si_2O_7$ phase. Absorption spectra revealed low bandgap and high Urbach energy values indicating improved crystallinity in the glass network. The luminescence lifetime of Sm^{3+} in the $Sm_2Si_2O_7$ crystal phase was slightly longer than that in precursor glass indicating successful doping. The color coordinates revealed reddish-orange emissions indicating potential applications in lasers and LEDs.

Alhodiab et al. [40] developed a glass from agro-food waste with a composition of $25SiO_2$-$30Na_2O$-$45B_2O_3$ (in mol%) ash by a melt-quenching technique where SiO_2 was extracted from rice husk. Further, it was doped with 4% Dy_2O_3 or Nd_2O_3. XRD patterns confirmed the amorphous nature of samples. Further, the emission spectra of the samples were studied to learn about the luminescence nature of glasses. Dy^{3+} doped samples emitted yellow and blue light which resulted in a white flash.

Truong et al. [41] prepared a variety of glasses having the composition $40SiO_2$–$25Al_2O_3$–$18Li_2O$–$7LiF$-$(10\text{-}x\text{-}y)YF_3$-$xEr_3$-$yYbF_3$ (in mol.%.), in which YF_3 was partially substituted by YbF_3 and ErF_3 by melt quenching method. Thermal treatment was performed at 540^{o}C for up to 80 h. XRD patterns confirmed the formation of $LiYF_4$ and $LiAlSiO_4$ nanocrystals. Two different lifetimes for green emission were identified in the sample i.e. a short lifetime (12-18 μs) and a long lifetime (110-160 μs). The red emission lifetimes of the doped glasses were longer as compared to the base glass, which makes them suitable for advanced photonic applications.

Teja et al. [42] synthesized a glass having the chemical composition $(60\text{-}x)Si_2O_3$- $20ZnO$- $15Li_2CO_3$ - $5Pb_3O_4$- xEu_2O_3 where (x=0.1, 0.2, 0.3, 0.4, 0.5 mol%). X-ray diffraction patterns confirmed their amorphous nature. These glasses had high density and refractive indices. They observed high-

intensity absorption peaks at 377 and 609 nm. As the europium ion concentration was increased, the energy band gap values decreased. CIE plots showed that when excited at 377 nm wavelength the glass samples emit white light. The glasses can be efficiently used to convert high-energy light into visible light with specific colors.

Monsiha et. al. [43] fabricated base glass with composition $20SiO_2$-$(20-x)B_2O_3$-$10Al_2O_3$-10ZnO-30NaF-$10ZnF_2$-xEu_2O_3 where x= 0.1, 0.5, 1.0, 1.5, 2.0 and 2.5 mol% by melt quenching technique. After heat treatment, crystallization is observed in the samples. The indirect band gap around 4 eV is appropriate for LED and laser applications. CCT values revealed that they emit red color so are suitable for red laser.

Mirdda et al. [44] synthesized pure and Pr^{3+} doped Na_2O-ZnO-TeO_2 glasses using the melt quenching method. With the increase in the concentration of Pr^{3+} ions, an increase in the value of the refractive index is observed. In contrast to this, the value of optical bandgap decreases. Even the intensity of peaks in the emission spectra increased with higher concentrations of Pr^{3+} ions, which makes them suitable for optical purposes.

Liu et al. [45] developed a series of Pr^{3+}- doped SiO_2–Al_2O_3–Na_2O-NaF-YF_3 (SANYF) glasses using a conventional melt quenching technique. Introduction of Pr_2O_3 disturbed the glass matrix reducing band gap from 3.66 eV to 3.42 eV. Glass samples were subjected to thermal temperature at 690^oC for 1 h which led to the formation of $Na_5Y_9F_3$ nanocrystals. Under 443 nm light excitation samples exhibited the strongest luminescence. The luminescent characteristics nominate the glasses for application in both up conversion and down conversion.

Maity et al. [46] synthesized Eu^{3+}-Tb^{3+} co-doped titanium zinc sodium phosphate glass. The glass composition was $1Eu_2O_3$-$1Tb_2O_3$-$4TiO_4$-14ZnO-$20Na_2O$-$60P_2O_5$ (mol%). XRD patterns revealed the amorphous nature of samples. The energy transfer between Eu^{3+} and Tb^{3+} ions was confirmed by emission and excitation spectra. It was observed that by varying excitation wavelengths different colors are emitted and confirmed that the glass can be utilized in photonics, W-LED and display devices.

2.1. Motivation for the present study: -

Based on the above discussion, it can be concluded that glasses and glass-ceramics can be used as phosphors for photoluminescence applications. From the literature, it is clear that limited work is available on agro-food waste-derived glass-ceramics as a phosphor is used for the photoluminescent properties. Very few reports on the use of rice husk and eggshell for the synthesis of phosphor for photoluminescent applications are present. The use of hybrid sources i.e., agro-food waste sources with other conventional chemicals to synthesize glass and its conversion into glass-ceramics for the

photoluminescent applications is not explored yet. Based on the above discussions, the following objectives are decided for the present research work.

2.2. Objectives:

1. Synthesis of glass using agro-food waste with $43SiO_2$-$24.5CaO$-$24.5Na_2O$-$7P_2O_5$ (wt%) and conversion to glass-ceramics with the doping of 0.5 wt% of rare-earth ions (Dy^{3+}, Eu^{3+}, Sm^{3+}, and Pr^{3+}).
2. To study their structural, optical, and photoluminescent properties using various characterization techniques.

Chapter 3 Materials and Methods.

This chapter presents the details of the methods used for the synthesis of the glass from agro-food waste followed by the synthesis of glass-ceramics with the addition of the different rare earth elements such as Eu^{3+}, Sm^{3+}, Dy^{3+}, and Pr^{3+}. In the present work, a glass sample is synthesized by using the melt-quench. Further, the glass-ceramics with the addition of rare earth elements were synthesized using heat treatment. X-ray diffraction is used to identify the phase and determine particle size. Fourier-transform infrared spectroscopy is used to study the change in the structural units associated with SiO_2 and phosphorus networks. Raman spectroscopy was used to get more insight into the structural changes in amorphous and crystalline phases. Scanning electron microscope-Energy dispersive spectroscopy is employed to get information regarding the topography of the sample and determine the sample's composition. Uv-visible spectroscopy is implemented to find the optical band gap of the present sample, and photoluminescence spectroscopy is used to investigate the luminescence behavior of present samples doped with different rare-earth elements.

3.1. Preparation of glass and glass ceramics

The glass samples were synthesized from the hybrid sources i.e., SiO_2 from rice husk ash and CaO from egg shells using a composition $43SiO_2$-$25CaO$-$25Na_2O$-$7P_2O_5$ (wt%). It has been already reported that rice husk has SiO_2 as its main constituent with 97% purity and eggshells with 98% purity, which is already reported in many reports [22]. For the present study, the rice husk ash was collected from the rice mill, and washed thoroughly with distilled water to get rid of the contaminates, further it was dried and burned to convert it into ashes. The ashes were then calcined at 1250^{o}C for 4 h, followed by another calcination at 1400^{o}C for 4 h, to extract pure silica.

For the CaO, the egg shells were assembled from the hostels of Thapar Institute of Engineering and Technology, Patiala. They were washed thoroughly with distilled water, followed by washing with 1 M HCL solution. Egg shells were further dried in the oven at 70^{o}C overnight. The biowaste-driven SiO_2 and CaO were mixed with other conventional chemicals i.e., Na_2O and P_2O_5 in the desired ratio, and the melt was held at 1550^{o}C for 0.5 h to homogenize, followed by quenching using two thick copper plates.

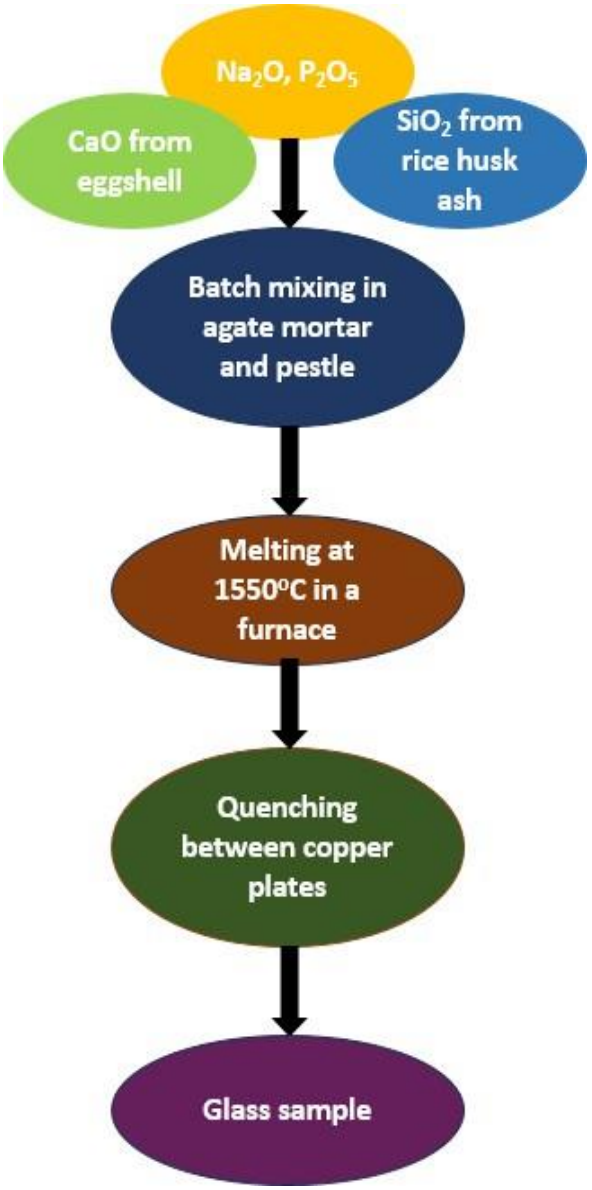

Fig. 3.1. Flowchart representing the glass preparation procedure

The glass sample was further grounded to powder form to add the rare earth elements in the 0.5 wt%. The samples were mixed in agate-mortar and pelletized in the size of 8 mm diameter, and 2 mm thickness using hydraulic press. Then the pellets were heat treated at 710°C i.e., the peak temperature of the glass sample (SC-0 glass reported in [47]) for 1 h and 10 h to convert them into glass-ceramics.

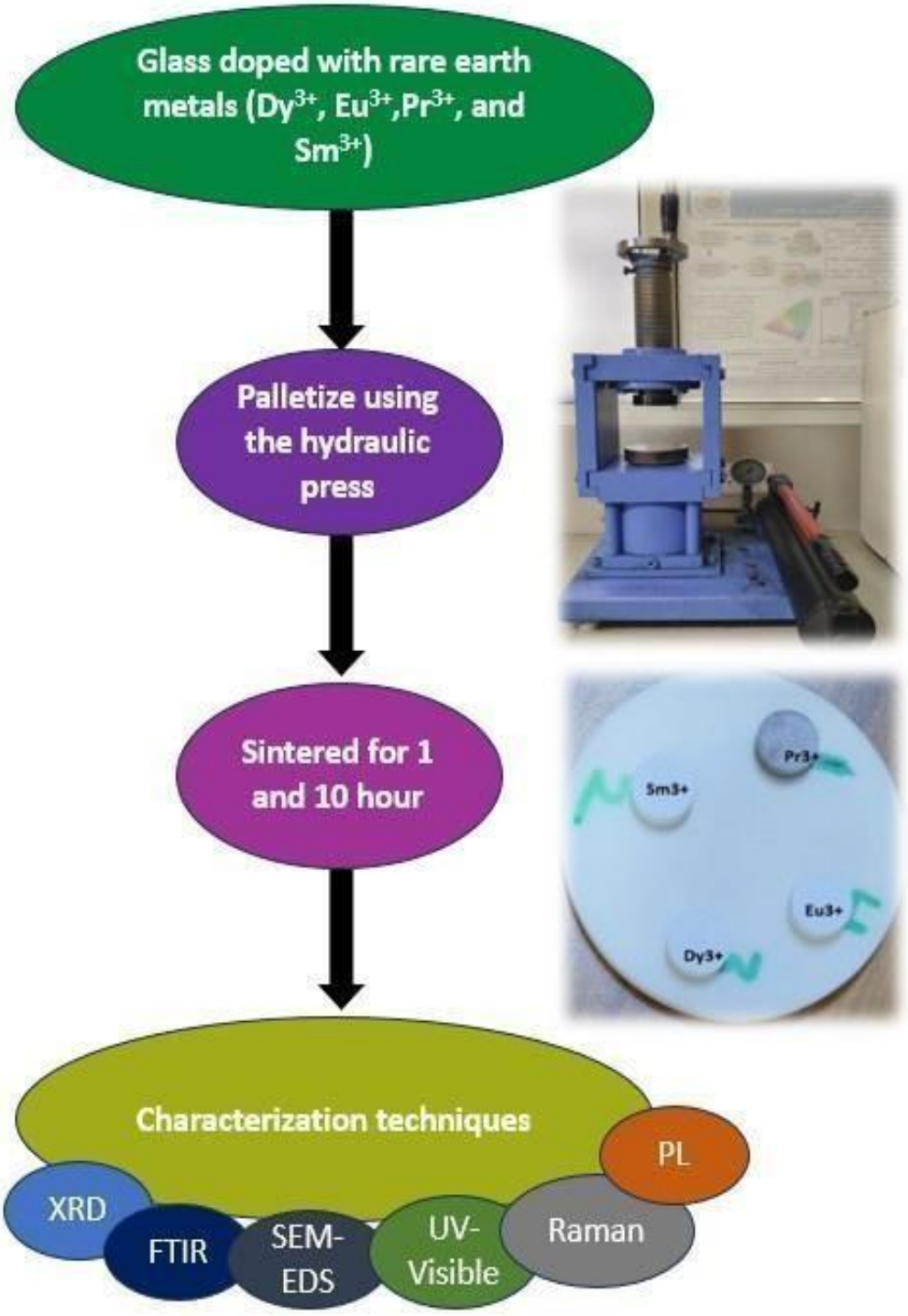

Fig. 3.2. Flowchart representing pellet preparation

3.2. Characterization techniques: -

3.2.1. X-ray diffraction

XRD analysis is a sophisticated technique in material science that is used to study crystallographic structure, phase composition, and physical properties of the materials. It gives information regarding phases formed, crystallite size, composition, lattice strain, inter-atomic distances, etc. XRD diffraction technique is based on the principle of interference specifically constructive interference of monochromatic X-rays and the light diffracted from the sample. The incident x-rays are diffracted at different angles from the sample but constructive interference is only observed for some specified angles. These specific angles should fulfill the condition of Bragg's law:

$$2dsin\theta = n\lambda \quad (1)$$

Where λ refers to the wavelength of X-rays incident on the sample, n is an integer, d is interplanar spacing and θ is the diffraction angle i.e. angle between the incident X-rays and atomic planes of the crystal.

It also provides information about the nature of the sample. For glasses or amorphous samples, instead of sharp peaks, broad humps or halos are observed. These broad humps indicate short-range order present in glasses. In the case of glass-ceramics, both sharp peaks and broad humps are observed. Sharp peaks correspond to the crystalline regions whereas the broad humps are for glass matrix. For this study, the XRD patterns of the glass ceramics were carried out on a PANalytical X'Pert PRO system (model: Rigaku Smartlab SE with hypix 400 2D detector) with CuKα source having a wavelength of 1.54Å. X-ray diffraction scattering range is generally kept in the range of 10-90^0. Further, these patterns are plotted and studied on X-pert high score software. This software matches the crystalline phases and peaks with the standard international centre of diffraction data (ICDD) card.

Using Debye Scherrer's equation, the crystallite size (D) of the crystal can also be determined.

$$D = \frac{K\lambda}{\beta cos\theta} \quad (2)$$

Where K is a dimensionless shape factor (about 0.9), λ refers to the wavelength of the monochromatic X-ray used, θ is for Bragg's angle and β is the associated XRD's peak full width at half maximum (FWHM).

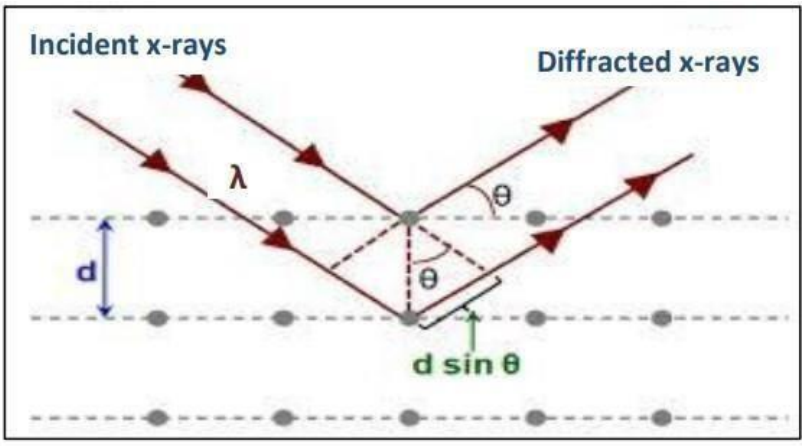

Fig. 3.3. Principle of X-ray diffraction analysis [48]

3.2.2. Scanning electron microscopy/energy dispersive spectroscopy (SEM/EDS)

SEM and EDS are distinct but complementary techniques. SEM is a powerful characterization technique to extract topographical, morphological, and crystallographic information about the sample. SEM produces images of high resolution to characterize a broad variety of specimens. To acquire point-by-point chemical and structural characteristics, an intense electron beam is used. The images of the sample are captured by scanning it with a high-energy beam of electrons in a raster scan pattern. This beam of electrons is produced by electron guns which may be either tungsten (W) or lanthanum hexaboride (LaB_6) filament. The sample and the electrons interact to generate signals that contain insights about the sample. When SEM is used the electron optical column and sample chamber must always be kept at a high vacuum of 10^{-3} to 10^{-4} Pa. SEM instrument consists of a source, two condenser lenses, two apertures, scan coils, an objective lens, and a detector. SEM JEOL 6700F high-resolution instrument was used to record scanning electron micrographs.

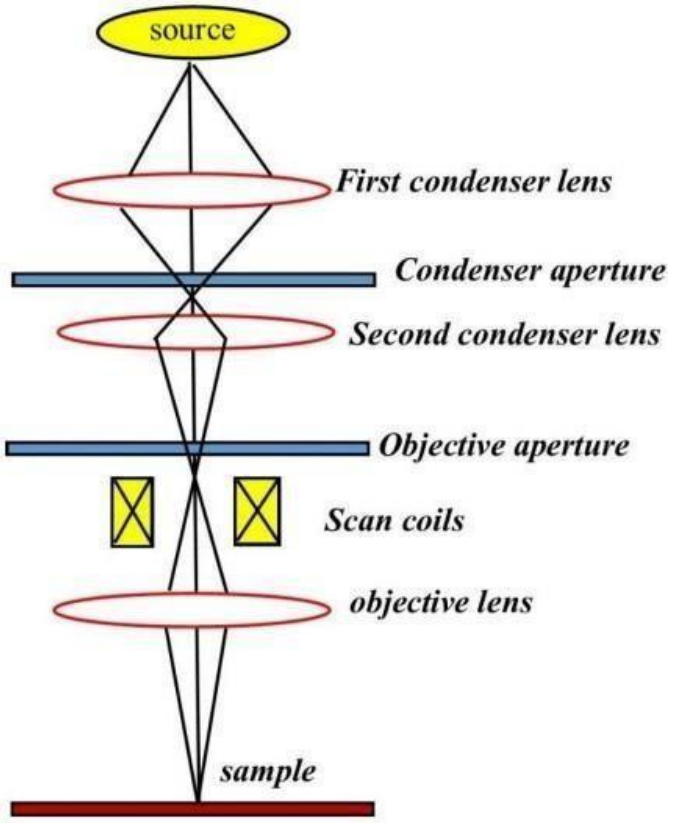

Fig. 3.2 Ray diagram of SEM

The various types of signals produced by the sample include x-rays, auger electrons, primary backscattered electrons, cathodoluminescence, secondary electrons, and specimen current. SEM detects the backscattered and secondary electrons to give surface morphology and topography. EDS is used to identify the elements (often in weight percent or atomic percent) present in the sample. EDS detects the X-rays to give information about elemental composition and its distribution.

3.2.3. Fourier transform infrared spectroscopy (FTIR)

Fourier transform infrared spectroscopy is a vibrational spectroscopic technique used to characterize the chemical bonds present in glass-ceramics or any other substance. It is a study of the interactions between matter and IR radiations. Bonds are not rigid and can be assumed as springs with weight at each end vibrating with some unique frequency. When IR radiation falls on the sample then only some of it is observed. The frequency that matches the frequency of vibration of the bond is absorbed and produces an IR band. Since all the molecules have different compositions, we get different FTIR spectra. It is carried out over a wide range of wavenumber i.e. 400-4000 cm^{-1}. Here, Fourier transform is used to transform the signal from the time domain to the frequency domain to obtain the final spectrum.

Michealson interferometer is used in FTIR spectrophotometers. The two mirrors are fixed at 90^0 to each other. For light, the He-Ne laser is used. Half of the light from the source is reflected at 90^0 and hits a fixed mirror, while the other half passes through the beam splitter and hits the moving mirror. The split beams recombine at the beam splitter after traveling different distances and thus exhibit an interference pattern. The detector collects the interfering signals when they pass through the detector and gives a plot. This plot is known as an interferogram.

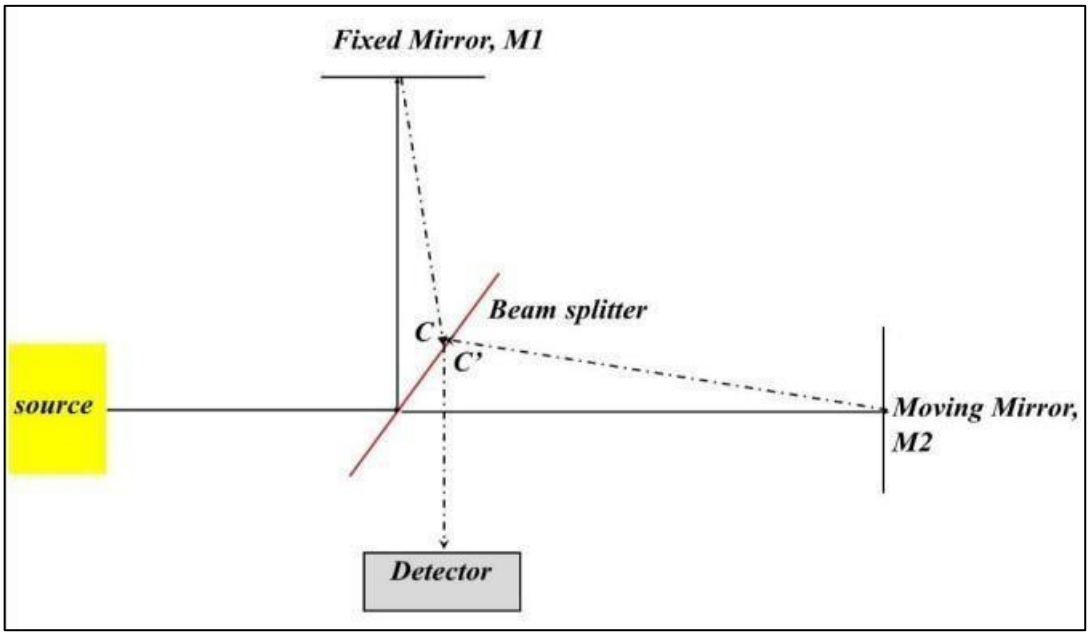

Fig. 3.5. Ray diagram of Michealson interferometer

Shimadzu Fourier transform infrared (FT-IR) spectrophotometer (model: IRTracer-100) was used to record infrared characteristic bands of various samples in the range of 4000–400 cm^{-1}. The infrared transparent chemical used for FTIR measurement was KBr.

FTIR spectrum is categorized into two regions:

1. Functional group region
2. Fingerprint region

The functional group region covers the range of 4000 cm^{-1} to 1450 cm^{-1}. Within this region, peaks are associated with the vibrations of functional groups attached to the molecules. It provides information about chemical bonds within a molecule. It is like a functional group signature. The fingerprint region covers the region below 1450 cm^{-1}. It contains a complicated series of bands which are due to different vibrations of the molecule. This region is used to identify the compound by comparing it with known references.

3.2.4. Raman spectroscopy

It is a technique used to study vibrational, rotational, and other low-vibration modes in a system. It is based on the principle of inelastic scattering of monochromatic light, typically a laser source. For silicate glasses, it helps to identify the formation of silicon-oxygen stretching vibrations, structural units of orthosilicate, inter-tetrahedral Si-O-Si linkages, and structural unit Q_{si}^{n} [49]. It also gives information regarding uniform glass-ceramics [50]. The laser beam is irradiated on the sample and it interacts with the molecules of the sample. On interaction with laser, a change in the polarizability of the sample is noticed. Raman bands arise due to this change in polarizability [49]. Due to this, the energy of the photons either increases or decreases. This difference provides information regarding the vibrational modes of the sample. The scattered frequency is of three types:

1. Rayleigh Scattering: If a molecule with no Raman-active modes absorbs phonon of frequency ν_0 then it will emit the phonons back with the same frequency ν_0. This interaction is known as Rayleigh scattering.
2. Stokes scattering: When the molecule has Raman-active modes then a change in the frequency of emitted light is absorbed. If the molecule absorbs energy from the phonon, then the scattered light has lower energy than the incident light. So, the frequency of incident light will be ν_0 while the frequency of scattered light will be ν_0-ν_m. This Raman frequency is referred to as Stokes frequency and interaction is known as Stokes scattering.
3. Anti-Stokes scattering: If the molecule is already in an excited vibrational state, then this type of interaction is observed. Molecules release extra energy to return to the basic vibrational state increasing the energy of scattered light. So, the light incident with frequency ν_0 is scattered with frequency $\nu_0+\nu_m$. This interaction is known as Anti-stokes scattering.

About 99.999% of the incident photons undergo Rayleigh scattering and do not provide any useful information. Only about 0.001% undergo Stokes or Anti-Stokes scattering which gives information about the vibrational modes of the molecule. For the present study, the Raman spectra (model: LabRAM HR EVO, France) were recorded in the 400-3750 cm^{-1} range, with a diode laser (532 nm) as the excitation source.

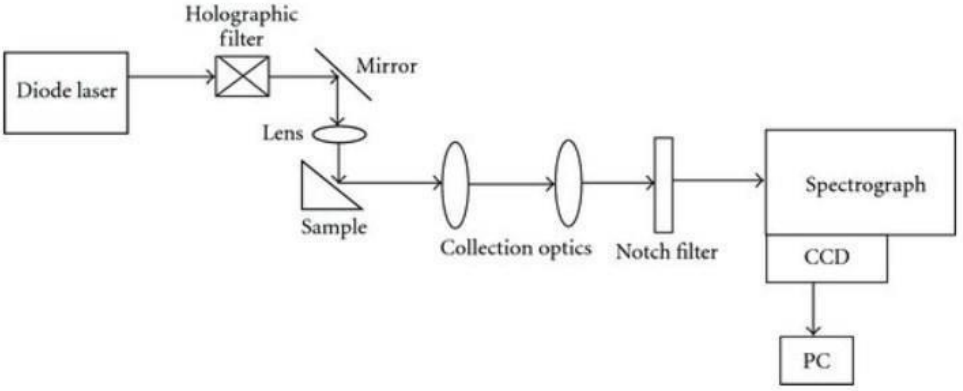

Fig. 3.6. Schematic diagram of Raman spectrometer

It can evaluate a broad variety of substances including solids, liquids, and gases. A plot of the intensity of scattered light versus Raman shift is extrapolated known as the Raman spectrum. The peaks in this spectrum correspond to different vibrational modes of the molecules in the sample.

3.2.5. Optical bandgap

The optical bandgap is a fundamental property of materials. It refers to the energy difference between the highest filled state of the valence band and the lowest unoccupied state of the conduction band. No electronic states exist in this range. It is a key parameter for determining the optical properties of the material. The most common method of determining optical bandgap is UV-visible spectroscopy. It is a reliable technique used to measure the reflection, transmission, and absorption of ultraviolet and visible light by a sample. A dual beam UV-visible diffused reflectance spectrophotometer was used to assess the bandgap for glass ceramic samples between the wavelengths of 200 and 800 nm (model: HITACHI U-3900 H).

Diffused reflectance spectra of all the samples are recorded. From these spectra, the optical band gaps are calculated using the Kubelka-Munk function. Kubelka-Munk function is defined as:

$$F(R) = \frac{(1-r)^2}{2r} = \frac{K}{S} \qquad (3)$$

The parameters F(R) refer to the Kubelka-Munk function, r is for reflectance, K is the absorption coefficient and S is the scattering coefficient. For direct bandgap, a graph between $(F(R)h\nu)^2$ and $(h\nu)$ is plotted while for indirect bandgap, $(F(R)h\nu)^{1/2}$ versus $(h\nu)$ graph is extrapolated. To get the value of the bandgap, a tangent is drawn from the curves to meet the x-axis. The values at which they cut the x-axis give the optical bandgap.

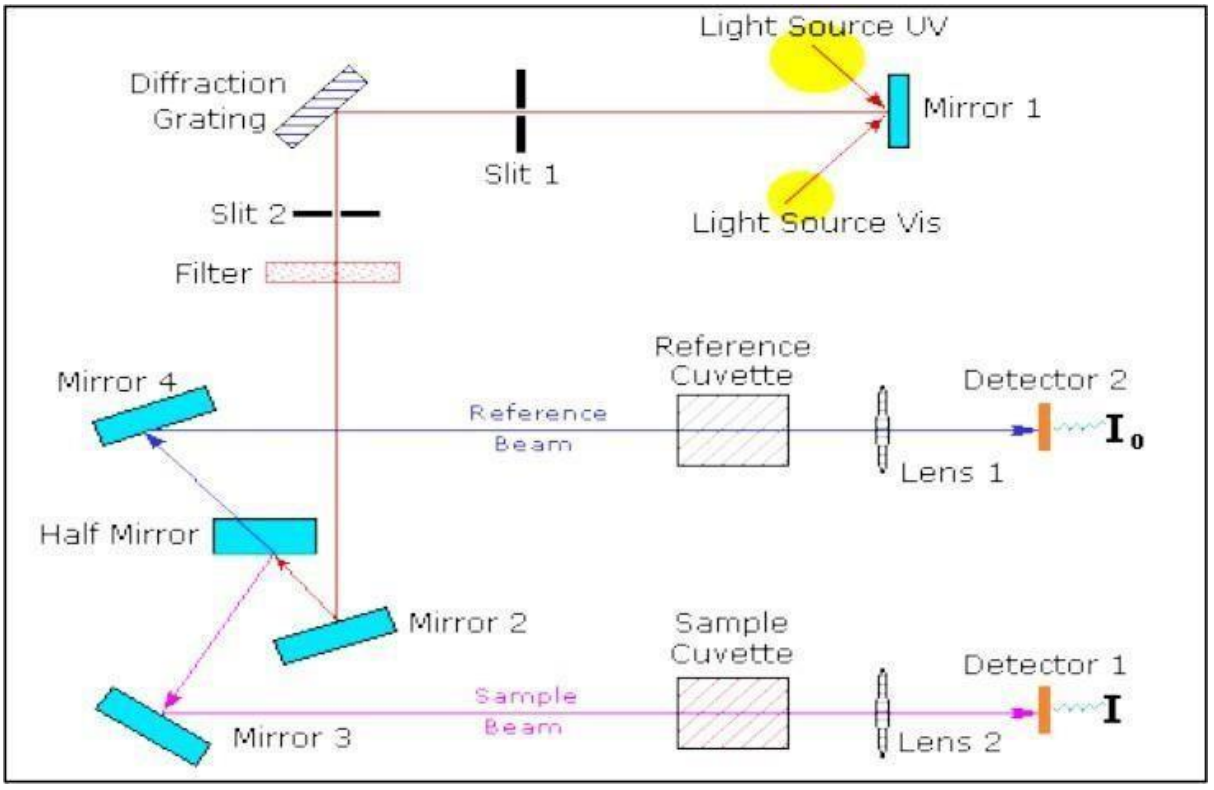

Fig. 3.7. Block diagram representing UV-Visible spectrophotometer [51]

3.2.6. Photoluminescence

Photoluminescence is used to study the luminescence behavior of the material. When light is incident on the sample, it gets absorbed by the sample. If the energy of the photon is greater than the bandgap of the material then the electrons get excited. These excited electrons move from the valence band or lower levels to higher excited levels. Eventually, these electrons return to lower energy to attain stability. During this process, they emit the energy of different wavelengths forming the emission spectra or PLE. The photoluminescence spectra were recorded using the Raman spectrometer using a He-Cd laser (at λ=325 nm) at room temperature.

4.1. XRD analysis:

The XRD analysis of all the prepared samples has been done. The XRD plot of the glass sample indicates the presence of a broad halo at 30°, which indicates the formation of the glasses, and is already reported in [47]. Further, all the heat-treated glass samples at 1 hr and 10 hr indicate the presence of sharp crystalline peaks in the spectra. It is observed that all the samples exhibit a similar phase, i.e. sodium calcium silicate phase. The majority of the peaks match with ICDD card no. 01-075-1686 ($Na_4Ca_4(Si_6O_{18})$) having rhombohedral structure. The formation of a similar phase in all the samples corresponds to the same base glass composition used for the synthesis of glass-ceramics with the doping of rare earth metals, that are used in low concentrations i.e. 0.05wt%. No additional peak for any of the rare earth metals is observed which means that they are well incorporated into crystal lattice [38].

The average crystallite size of the samples is determined by the Debye Scherrer's equation as given in Chapter 3 (section 3.2.1. eq. no. 1). Average crystallite size values for SND-1 and SND-10 are 36.11 nm and 46.35 nm; for SNE-1 and SNE-10 are 33.18 nm and 35.53 nm; for SNP-1 and SNP-10 are 31.18 nm and 43.87 nm; for SNS-1 and SNS-10 are 47.01 nm and 41.45 nm respectively. Dy^{3+}, Eu^{3+} and Pr^{3+} doped glasses follow the same trend. Their crystallite size increases with an increase in the sintering time. This is due to the increase in time for nucleation to occur, resulting in an increase in the crystallinity and the particle size [52]. It concludes that the heat treatment at 10 h favors better crystal growth as compared to those heat treated at 1 h.

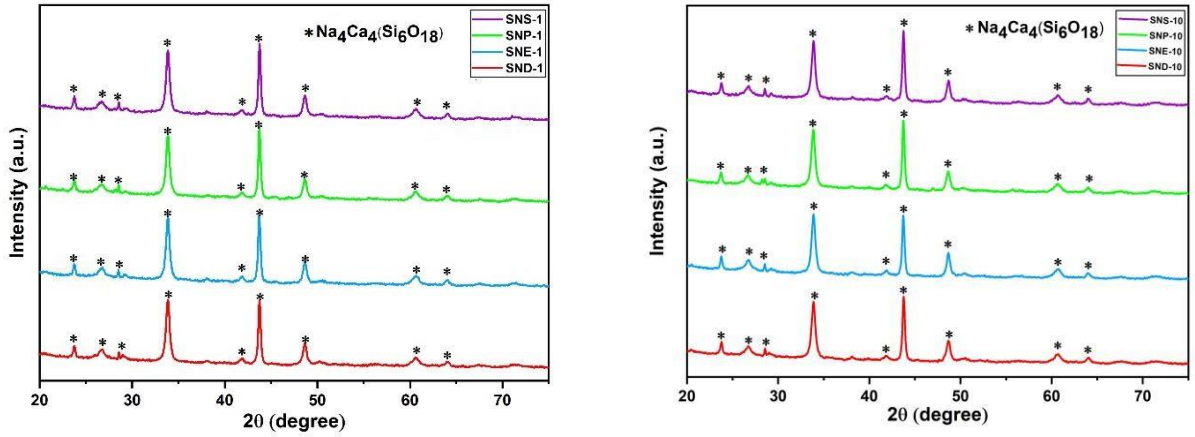

Fig. 4.1. XRD patterns of samples sintered for (a) 1 h and (b) 10 h after the addition of Dy^{3+}, Eu^{3+}, Sm^{3+}, and Pr^{3+} in the glass.

4.2. FTIR

FTIR spectra for glass ceramic samples sintered for 1 h and 10 h are shown in Fig.4.2. The FTIR spectra indicate the presence of almost similar bands in all the samples heat treated for 1 h and 10 h with the addition of rare earth metal ions. The bands corresponding to the silicate symmetric-asymmetric stretching as well as the bands associated with the phosphorus structure unit fall in the range of 800-1200 cm^{-1} [54-57]. The band observed at 1439 cm^{-1} is due to $C\text{-}O^{-}$ stretching of the carbonate bond as a minor amount is present in the glass sample, which is associated with the carbonyl group in the pores of eggshell [53-56].

Further, the peaks are deconvoluted to better understand the structural units. In the case of glass-ceramics with the addition of Dy, the deconvoluted spectra indicate the presence of bands at 1074, 1029, 1001, 918, 849, 695, 610, 510, and 430 cm^{-1}. The deconvoluted FTIR spectra can be divided into two parts i.e. 800-1000 cm^{-1} and 525-400 cm^{-1}. Chinna et al. [56] reported that these bands represent $Si\text{-}O^{-}$ stretching (ν_1, ν_3) and O-Si-O bending (ν_2, ν_4) modes respectively. The bands present in the range 610-700 cm^{-1} are because of the combined effect of the Si-O-Si stretching mode [54- 56]. Mattu et. al. [47] reported that the additional bands observed in the region 445-466 cm^{-1} and 503- 516 cm^{-1} represent the bending and rocking motion of SiO_4^{-} tetrahedral units. The bond observed at 576 cm^{-1} corresponds to asymmetric $P\text{-}O^{-}$ bending vibrations [57]. This FTIR spectra indicated no change in the spectral bands with the addition of different rare-earth metal ions. This may be due to the presence of rare-earth metal ions in very low concentrations in the present samples. However, with the increase in the heat treatment duration, the bands corresponding to the Si- O-MO (MO=Na_2O, CaO) bond increase, indicating the formation of the crystalline phase in the glass matrix, which is also supported by the XRD pattern of the heat-treated samples.

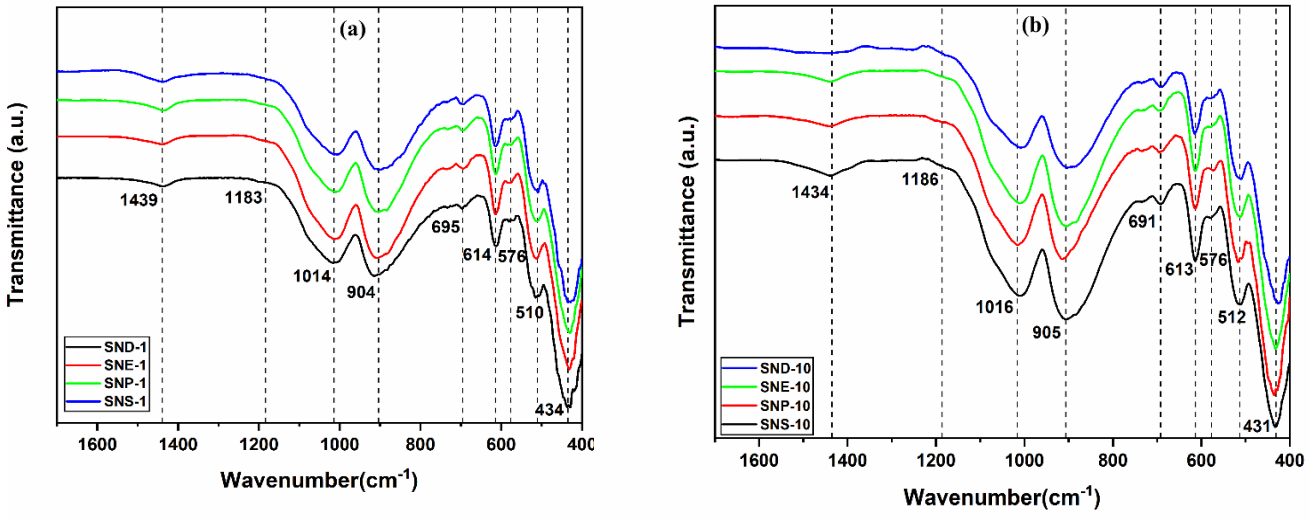

Fig.4.2. FTIR spectra of samples sintered for (a)1 h and (b)10 h

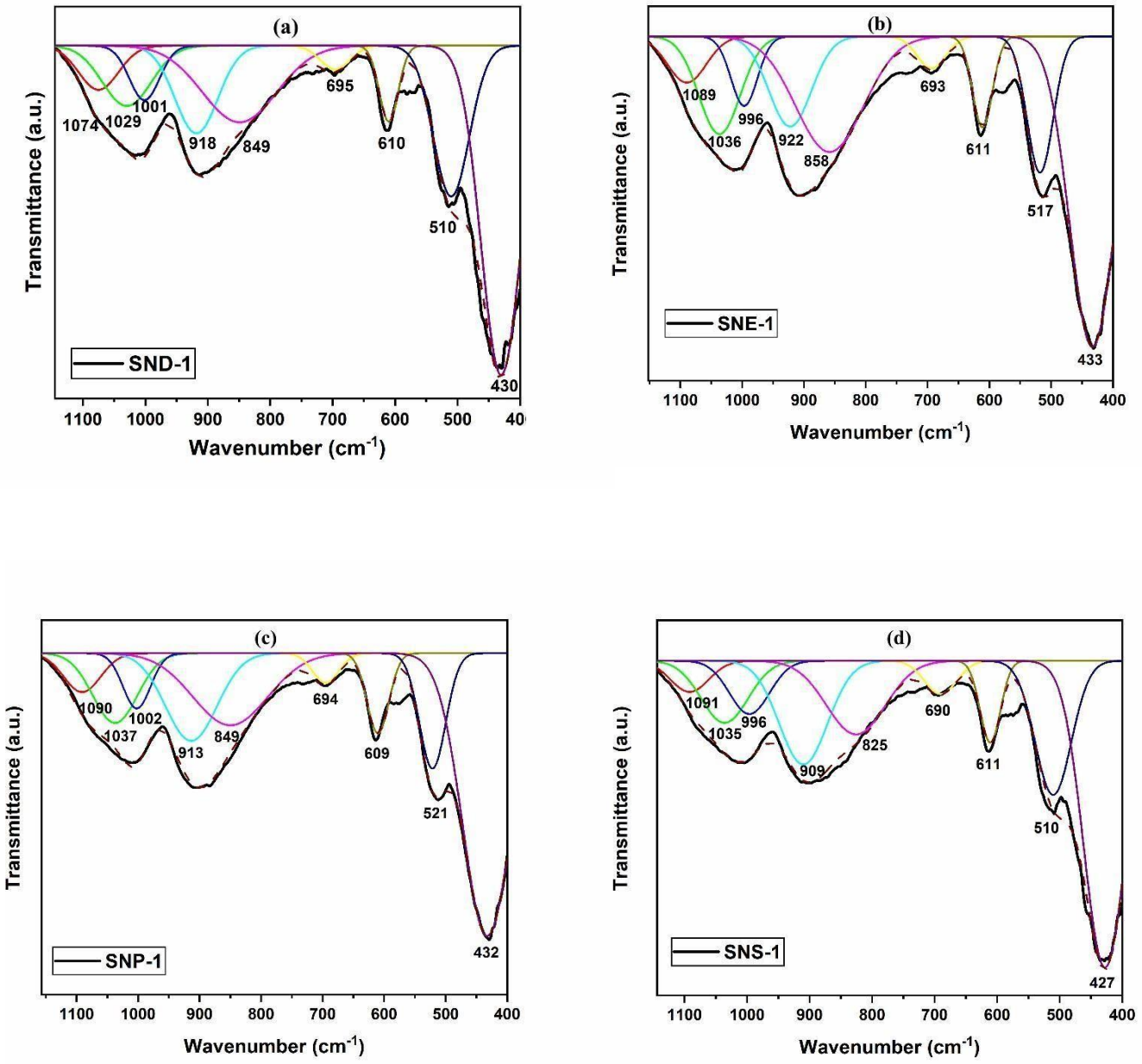

Fig.4.3. Deconvoluted FTIR spectra of (a) Dy^{3+}, (b) Eu^{3+}, (c) Pr^{3+}, and (d) Sm^{3+} doped glasses sintered for 1 h

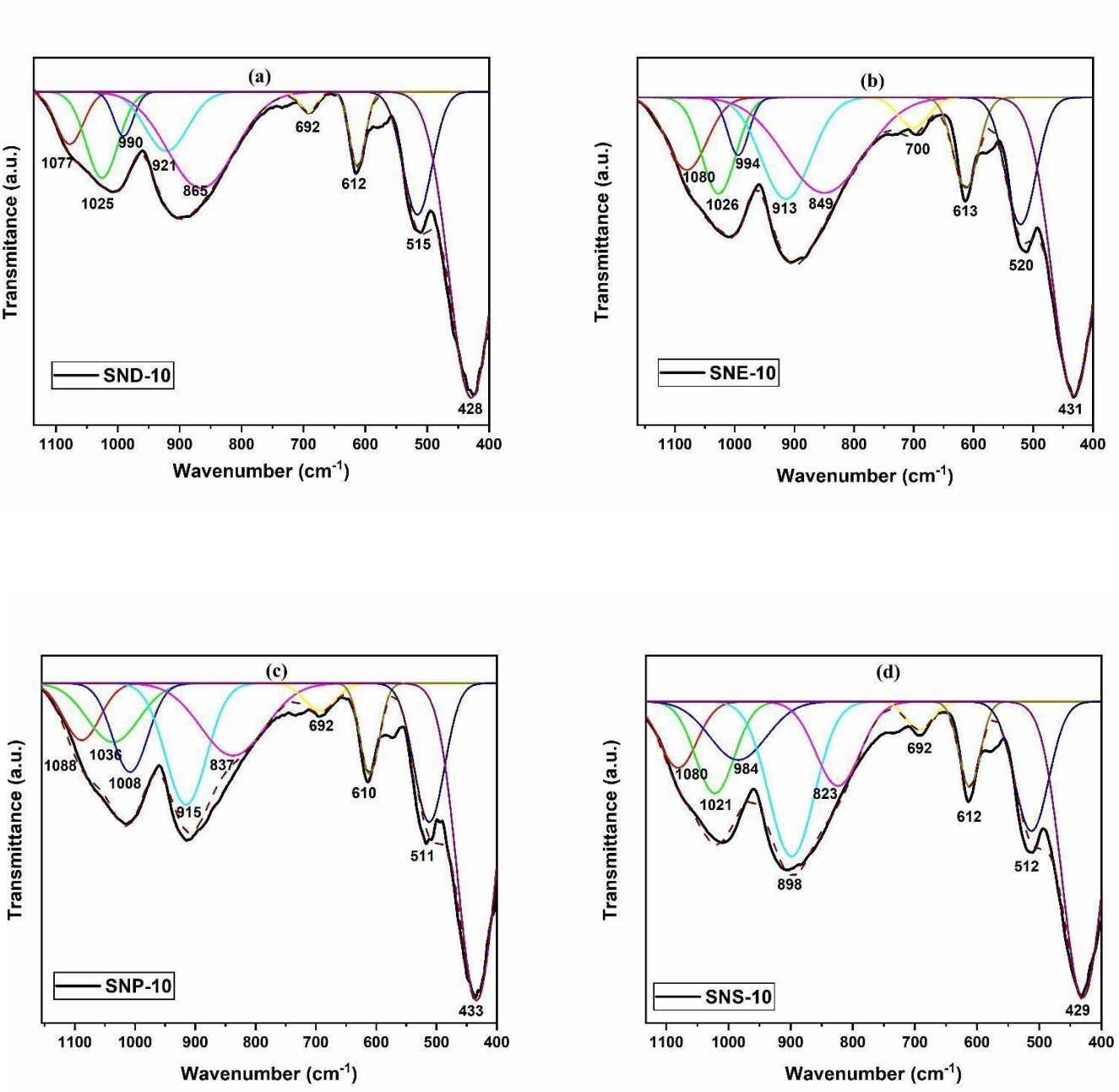

Fig. 4.4. Deconvoluted FTIR spectra of (a) Dy^{3+}, (b) Eu^{3+}, (c) Pr^{3+}, and (d) Sm^{3+} doped glasses sintered for 10 h

4.3. Raman analysis

Raman spectra of all the glass-ceramics are shown in Fig. 4.5. As similar to FTIR, Raman also indicates the presence of similar peaks in the spectra. The peaks located in the range 520-590 cm^{-1} are due to O-Si-O symmetric stretching [36]. The high-intensity peaks observed in the range 940-990 cm^{-1} correspond to $Si-O^-$ asymmetric stretching [58]. This range favors the Si-O-MO (MO= Na_2O, CaO)

bond formation which leads to phase formation. No change was recorded in the Raman spectra, since doping was in a very small percentage, and all of the samples show conversion to the sodium calcium silicate phase, as confirmed by XRD.

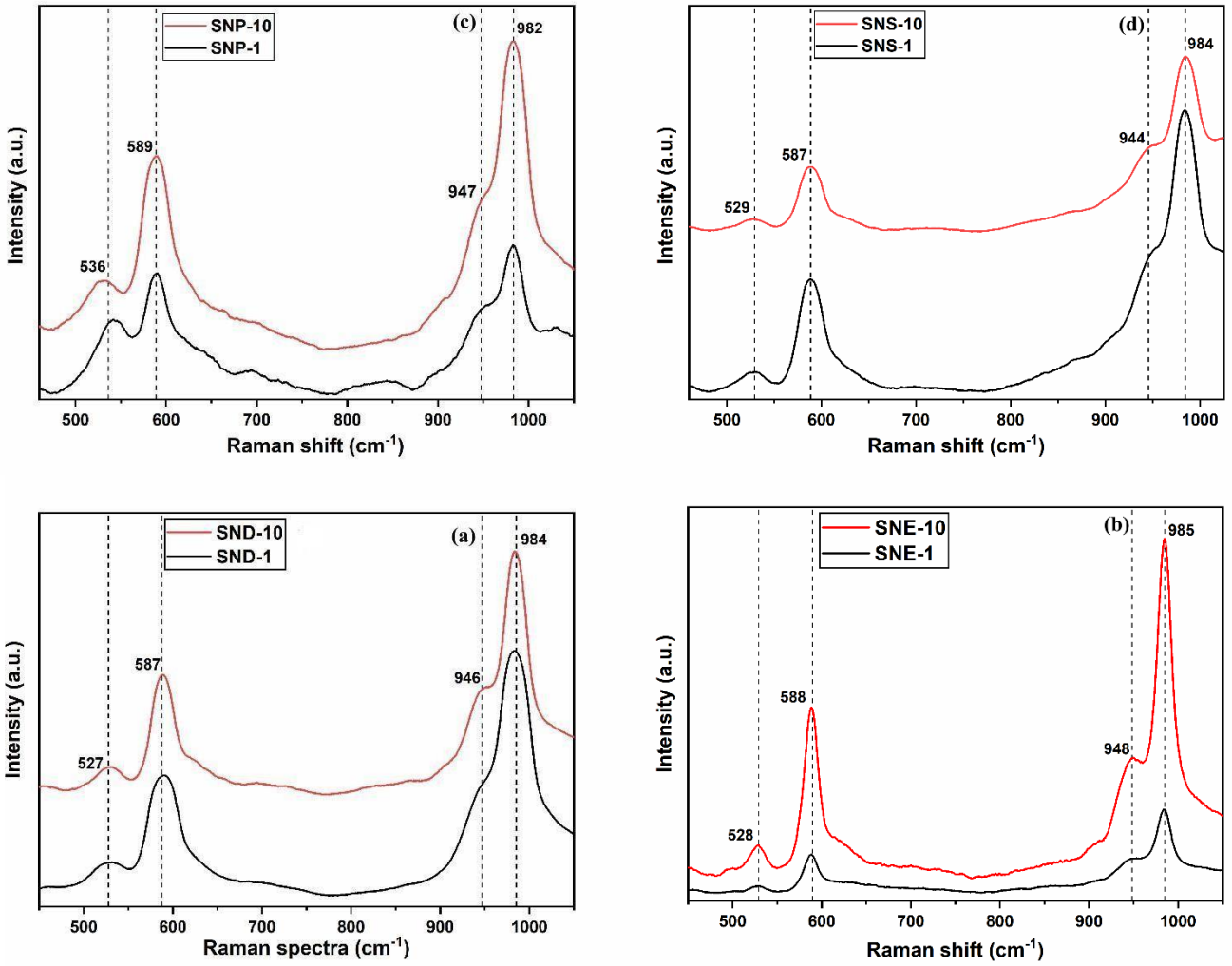

Fig. 4.5. Raman spectra of (a) Pr^{3+}, (b) Sm^{3+}, (c) Dy^{3+} and (d) Eu^{3+} doped glasses sintered for 1 h and 10 h

4.4. SEM-EDS analysis

SEM examination was used to determine the morphology of the samples. SEM images of SND and SNE are shown in Fig. 4.6. It is observed that the sodium calcium silicate phase is formed with crystals of rare earth metals embedded between them. Rare earth metals are not completely diffused into the glass matrix, because the melting point of the rare earth is very high [59-61], and the sintering temperature was not sufficient enough to completely diffuse them in the glass structure. However, it is evenly distributed in the composition. To study the elemental composition of samples EDS was

done. The sample contains Ca, O, Mg, Si, P, C, and respective rare earth metals doped into it. Carbon is present as carbon tapes were used during the mounting of the samples during analysis, and also present in very minute amounts in the samples, as explained in FTIR analysis.

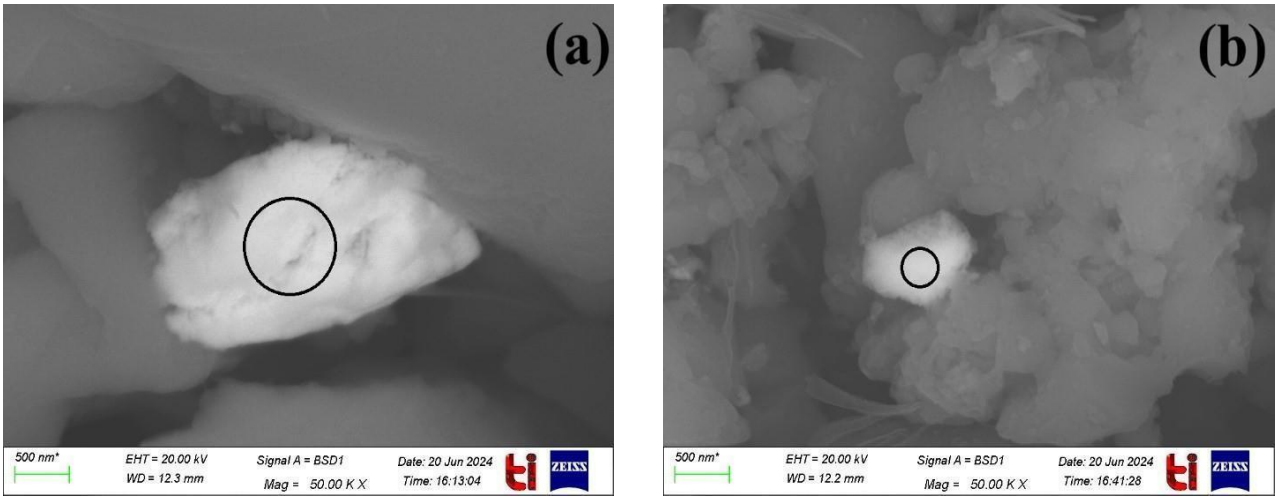

Fig. 4.6. Representative SEM images of (a) SND-1 and (b) SNE-1

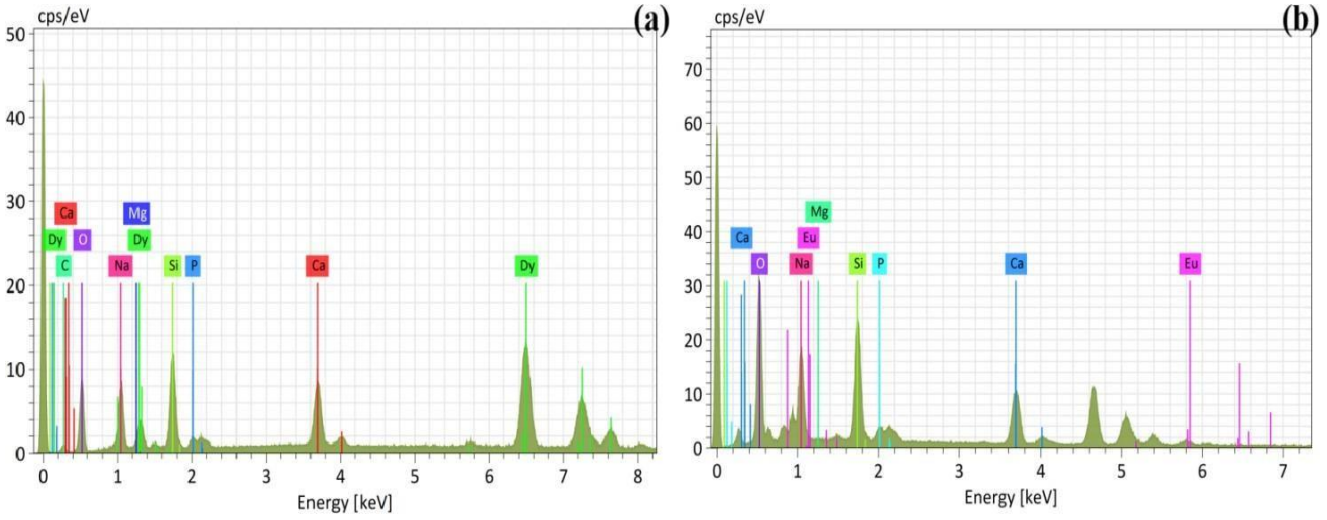

Fig. 4.7. Representative EDS images of (a) SND-1 and (b) SNE-1

4.5. Optical band gap

The reflectance spectrum of the glass-ceramics was recorded. The band gap is calculated in all the samples using the Kubelka-Munk function as given in Chapter 3 (section 3.3.5; eq. no. 3). The energy bandgap is defined as the energy difference between the highest occupied level i.e. valence band and the lowest empty band i.e. conduction band.

The plots of $(F(R)h\nu)^2$ vs energy hν are extrapolated and a tangent is extended from each curve as shown in Fig. 4.8. The point at which the tangent meets the x-axis gives the value of the optical bandgap. The values of band gaps of different samples heat treated for different time durations are given in Table 1. It is observed that Eu^{3+} doped glass-ceramics exhibit the highest value of energy bandgap. It should be noted that the optical band gap of the base glass is 3.9 eV. The formed glass-ceramics have a lower bandgap than the base glass. The degree of structural order-disorder in the lattice can be the reason behind this variation, as it directly influences the distribution of intermediate energy levels within the bandgap [62]. Also, with an increase in heating duration, the band gap energy of all the samples shows a decreased value at 10 h as compared to 1 h, which indicates the reflectivity is decreased in all the samples, with the increase in the crystallization tendency, which may be due to the increased growth of $Na_4Ca_4(Si_6O_{18})$ phase resulting into new defects and large energy levels between their valence and conduction bands that decrease the optical band gap [63]. The band gap in this range is also reported in the literature for the calcium silicates [56]. These results indicate that the bandgap of all the samples lies in the semiconductor range, and can be used for the dielectric materials.

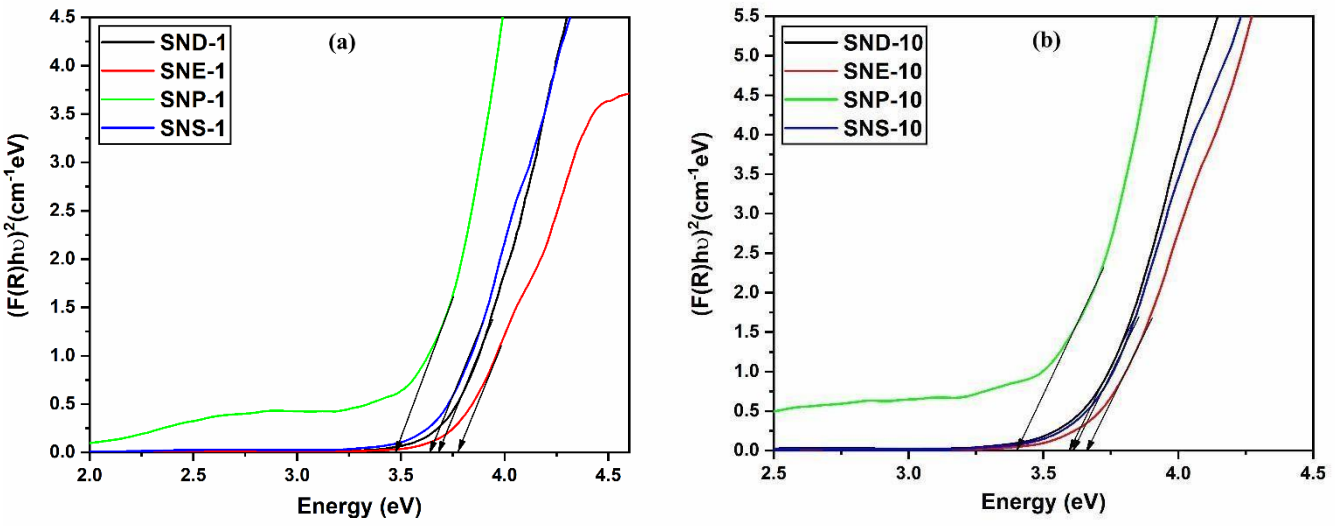

Fig. 4.8. Optical band gap of samples sintered at (a)1 h and (b) 10 h

Table 1

Values of direct band gap for glass-ceramics

Sample	Band gap (eV)
SND-1	3.67
SND-10	3.59

SNE-1	3.76
SNE-10	3.65
SNP-1	3.47
SNP-10	3.39
SNS-1	3.63
SNS-10	3.60

4.6. Photoluminescence spectra

Photoluminescence spectra of all the synthesized samples are recorded at excitation wavelength λ_{ex}=325 nm.

The PLE spectrum of SNS sample is shown in Fig.4.9 (a). The spectrum consists of five peaks in yellow (561 nm), orange (600-610 nm), orange-reddish (654 nm), and red (707 nm) regions. These peaks assigned to $^4G_{5/2}\rightarrow{}^6H_{5/2}$, $^4G_{5/2}\rightarrow{}^6H_{7/2,}$ $^4G_{5/2}\rightarrow{}^6H_{9/2}$ and $^4G_{5/2}\rightarrow{}^6H_{11/2}$ transitions respectively [64]. Maximum intensity peak is observed in the orange region. The transition at 561 nm is a purely magnetic dipole with selection rule $\Delta J=0$. The transition with maximum intensity in the range 600-610 nm is both magnetic and electric dipole in nature with selection rule $\Delta J=1$. The transitions at 654 and 707 nm are purely electric dipoles following selection rule $\Delta J\leq 6$ and $\Delta L=2$ [39]. Four emission peaks are observed in Fig. 4.9 (b). in Pr^{3+} doped samples. These peaks can be attributed to $^3P_0\rightarrow{}^3H_4$, $^3P_1\rightarrow{}^3H_{4,}$ $^3P_0\rightarrow{}^3H_5$ and $^1D_2\rightarrow{}^3H_4$ respectively [65]. A transition from $^1D_2$ level is observed and can be considered the cause of non-radiative transitions from $^3P_0$ level. The peaks at 484 and 604 nm correspond to non-radiative processes and excited states relaxation [42].

Fig. 4.9 (c). depicts the PLE of SNE in which five peaks are visible. The peaks located at 578, 593, 611, 653, and 703 nm belong to $^5D_0\rightarrow{}^7F_0$, $^5D_0\rightarrow{}^7F_1$, $^5D_0\rightarrow{}^7F_2$, $^5D_0\rightarrow{}^7F_3$ and $^5D_0\rightarrow{}^7F_4$ respectively [38]. All transitions arise from the same level $^5D_0$. The most intense peak at 611 nm originates from the electric dipole transition [66]. The transitions at 578 nm ($^5D_0\rightarrow{}^7F_0$) and 593 nm ($^5D_0\rightarrow{}^7F_1$) are magnetic dipole transitions. The transitions $^5D_0\rightarrow{}^7F_2$ and $^5D_0\rightarrow{}^7F_4$ are hypersensitive while the transition $^5D_0\rightarrow{}^7F_1$ is insensitive to the symmetry of Eu^{3+} [67]. In the case of the Dy^{3+} doped sample, four transition peaks are observed at 474, 482, 488, and 576 nm as shown in Fig. 4.9 (d). The peaks located in the range 460-500 nm are assigned to Dy^{3+} transition: $^4F_{9/2}\rightarrow{}^6H_{15/2}$ (blue) and the peak at 576 nm is because of transition $^4F_{9/2}\rightarrow{}^6H_{13/2}$ (yellow) [27]. The blue band is a magnetic dipole in nature while the yellow band is due to a forced electric dipole (hypersensitive) transition which obeys the selection rule i.e. $\Delta S=0$, $\Delta L=2$, $\Delta J=0$ [68]. It is observable that the intensity of the yellow band is

stronger than the blue band which confirms the presence of Dy^{3+} ions at no inversion centres [55]. The yellow emission is also beneficial to promote white light emission. It is observed that no shifting in peak position is recorded with an increase in sintering time in all the samples except intensity.

To characterize the color emitted by phosphors, Commission International de'Eclairage (CIE) chromaticity coordinates are studied. The color coordination points for all the rare earth-doped samples are shown in Fig 8. The CIE x and y coordinates are given in Table 1. The CIE values of S-0 glass sample lie in the greenish region, which may be due to any trace element present in the agro-food waste such as titanium, which is widely reported in the literature that titanium is present in rice husk in the very small amount [25], but no different peak of Ti was observed in EDS spectra, which may be due to its very minute percentage. However, with the doping of rare earth, it shifts to the blue region. Similar behavior was recorded in Dy^{3+} doped glass-ceramic $NaGd(WO_4)_2$ prepared by the melt quench method and subsequent heating [69]. Similarly, Sm^{3+}, Pr^{3+}, and Eu^{3+} lie in the same region i.e. orange-red region. There is minimal shifting with an increase in the duration of sintering time. To determine the coolness or warmth of the light, correlated color temperature (CCT) values are studied. The light sources with CCT values higher than 5000 K are known as cool sources, while the sources with values less than 5000 K are considered warm sources [68]. CCT values are calculated using McCamy's equation [70]:

$$CCT = -449n^3 + 3525n^2 - 6823n + 5520.33 \quad (1)$$

Where n is calculated by the formula given below:

$$n = \frac{x - x_e}{y - y_e} \quad (2)$$

Where x and y are the CIE coordinates and the values of x_e and y_e are 0.332 and 0.186 respectively. The calculated CCT values are tabulated in Table 2. For SNE-1, SNE-10, SNS-1, SNS-10, SNP-1, and SNP-10 the CCT values are calculated to be less than 5000 K thus they are warm sources whereas for other samples i.e. SND-1 and SND-10 CCT values are greater than 5000 K which means they are cool light sources [71]. The results indicated that the sodium calcium silicate phase derived from agro-food waste glasses/glass ceramics can be used as a phosphor for different color LED applications.

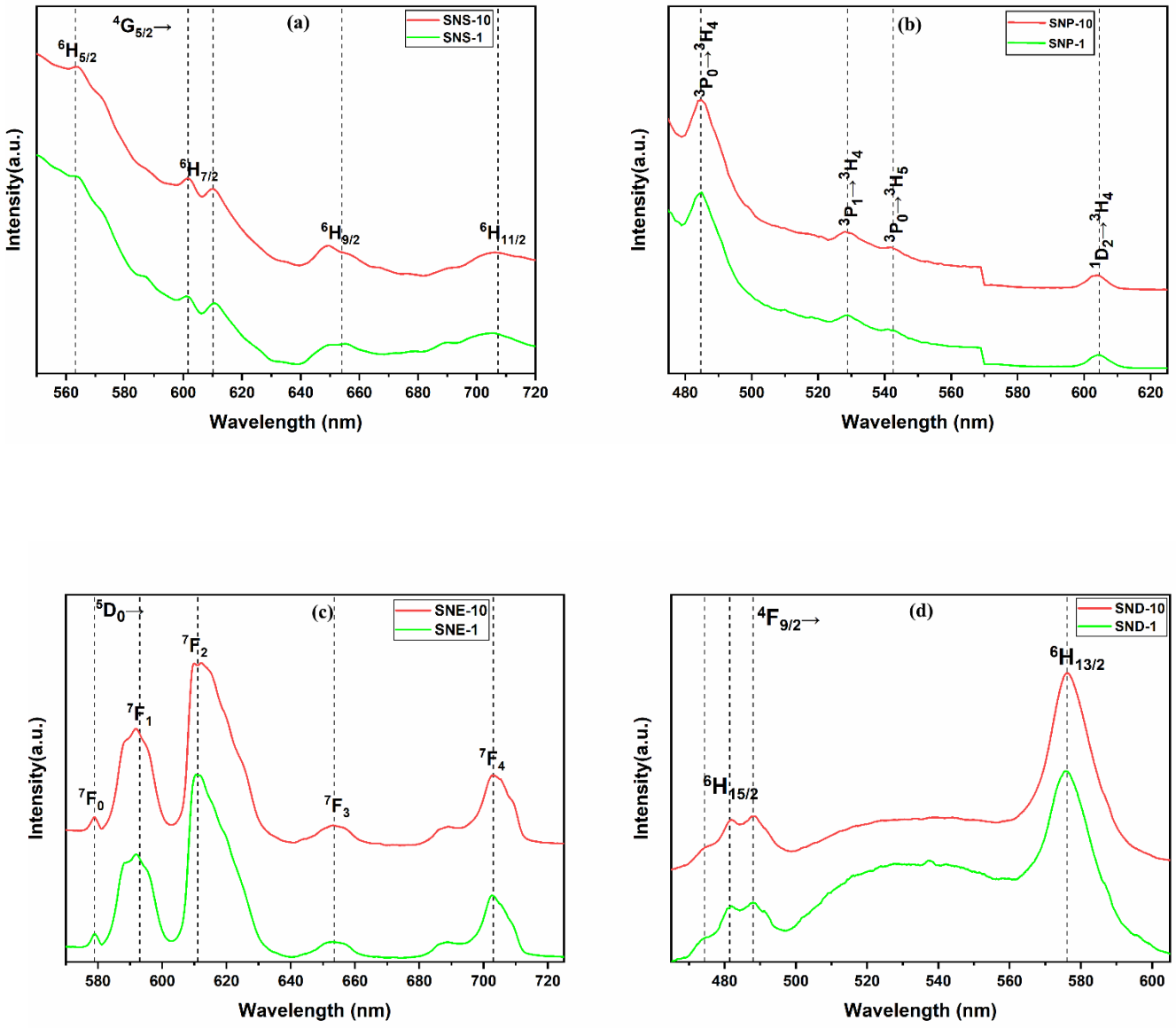

Fig. 4.9. PLE spectra of glass samples doped with (a) Sm^{3+}, (b) Pr^{3+}, (c) $Eu^{3+,}$ and (d) Dy^{3+}

Table 2

Values of CIE co-ordinates and CCT for all the synthesized glass-ceramics

Sample	CIE coordinates (x, y)	CCT (K)
SND-1	0.3066, 0.1967	47586
SND-10	0.3083, 0.1987	33446
SNE-1	0.5626, 0.4195	1788
SNE-10	0.5545, 0.4230	1851
SNS-1	0.6895, 0.3097	4405

SNS-10	0.5333, 0.4406	2107
SNP-1	0.5139, 0.4314	2216
SNP-10	0.5397, 0.4376	2037

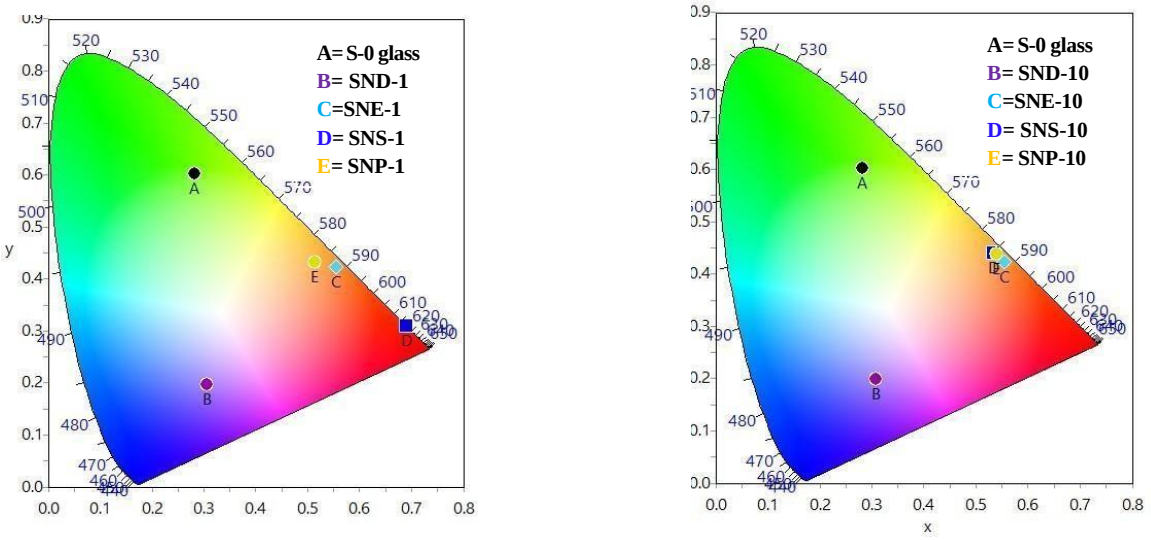

Fig. 4.10. CIE diagrams for glass samples sintered for (a) 1 h and (b) 10 h

Chapter 5 Conclusion.

5.1. Conclusion:

The glasses were synthesized successfully using hybrid sources i.e., SiO_2 and CaO from agro-food wastes mixed with other conventional chemicals in a desired composition using the melt quench technique. The glasses were further heat-treated for 1 h and 10 h to form glass-ceramics with the doping of different rare earth ions i.e., Sm^{3+}, Pr^{3+}, Eu^{3+}, and Dy^{3+}. The XRD results indicate the formation of sodium calcium silicate phase in all the glass-ceramics. The optical band gap for these glass-ceramic samples lies in the range of 3.76-3.60 eV, which decreases with increased sintering time. The CIE coordinates indicate the yellowish-green color for the undoped glass sample, and the blue color for the Dy^{3+}, and samples with Sm^{3+}, Eu^{3+}, and Pr^{3+} emit a red-orange color. The yellowish-green color of the glass sample is due to the presence of trace elements in the agro-food waste.

5.2. Future scope of the study:

The band gap of these synthesized glass-ceramics lies in the wide semiconductor range, indicating that these samples could be tested for moderate dielectric material applications. The photoluminescence and CIE study can be further conducted on the prolonged heat-treated glass to find out the effect of the formation of crystalline phases and their volume.

References:

1. J. E. Shelby, Introduction to Glass Science and Technology, Royal Society of Chemistry, Cambridge, 2nd edn., 2005.
2. Jiusti J, Zanotto ED, Feller SA, Austin HJ, Detar HM, Bishop I, Manzani D, Nakatsuka Y, Watanabe Y, Inoue H. Effect of network formers and modifiers on the crystallization resistance of oxide glasses. Journal of Non-Crystalline Solids. 2020 Dec 15;550:120359.
3. Calahoo C, Wondraczek L. Ionic glasses: Structure, properties and classification. Journal of Non-Crystalline Solids: X. 2020 Dec 1;8:100054.
4. Gy R. Ion exchange for glass strengthening. Materials Science and Engineering: B. 2008 Mar 25;149(2):159-65.
5. Khan S, Kaur G, Singh K. Effect of ZrO_2 on dielectric, optical and structural properties of yttrium calcium borosilicate glasses. Ceramics International. 2017 Jan 1;43(1):722-7.
6. Kaur N, Kaur G, Khan S, Singh K. Conductivity, dielectric, and structural studies of (30-x)SrO-xBaO-10Al_2O_3-45SiO_2-5B_2O_3-10Y_2O_3($5 \leq x \leq 25$) glasses. Ionics. 2018 Aug;24:2343-53.
7. Marker III AJ, Neuroth N. Overview Optical Glass: An Engineered Material. The Properties of Optical Glass. 1998:1-7.
8. Jha PK, Pandey OP, Singh K. FTIR spectral analysis and mechanical properties of sodium phosphate glass–ceramics. Journal of Molecular Structure. 2015 Mar 5;1083:278-85.
9. S.D. Stookey, Nucleation "Ceramic Fabrication Process, John Wiley, New York, 1960
10. S. D. Stookey, ‘‘Method of Making Ceramics and Product Thereof,’’ U. S. Patent 2920971, 1960
11. Sakamoto A, Yamamoto S. Glass-ceramics: engineering principles and applications. International Journal of Applied Glass Science. 2010 Sep;1(3):237-47.
12. Z. STRNAD, Glass-Ceramic Materials, (Elsevier, Amsterdam 1986).
13. Khater GA, Safwat EM, Kang J, Yue Y, Khater AG. Some types of glass-ceramic materials and their applications. International Journal of Research. 2020;7(4):1-6.
14. Deubener J, Allix M, Davis MJ, Duran A, Höche T, Honma T, Komatsu T, Krüger S, Mitra I, Müller R, Nakane S. Updated definition of glass-ceramics. Journal of Non-Crystalline Solids. 2018 Dec 1;501:3-10.

15. Karmakar B. Functional glasses and glass-ceramics: processing, properties and applications. Butterworth-Heinemann; 2017 Jun 8.

16. Alekseeva I, Dymshits O, Tsenter M, Zhilin A, Golubkov V, Denisov I, Skoptsov N, Malyarevich A, Yumashev K. Optical applications of glass-ceramics. Journal of Non-Crystalline Solids. 2010 Dec 1;356(52-54):3042-58.

17. Suzuki T, Horibuchi K, Ohishi Y. Structural and optical properties of $ZnO–Al_2O_3–SiO_2$ system glass–ceramics containing Ni^{2+}-doped nanocrystals. Journal of non-crystalline solids. 2005 Aug 15;351(27-29):2304-9.

18. Rawlings RD, Wu JP, Boccaccini AR. Glass-ceramics: their production from wastes—a review. Journal of materials science. 2006 Feb;41:733-61.

19. Shrivas A, Jain D, Joshi R. Application of different waste in concrete as a partial replacement of cement. Int. J. Sci. Technol. Eng. 2015 Sep;2:89-107.

20. Sankar S, Kaur N, Lee S, Kim DY. Rapid sonochemical synthesis of spherical silica nanoparticles derived from brown rice husk. Ceramics International. 2018 May 1;44(7):8720-4.

21. Lim JS, Manan ZA, Alwi SR, Hashim H. A review on the utilization of biomass from the rice industry as a source of renewable energy. Renewable and sustainable energy reviews. 2012 Jun 1;16(5):3084-94.

22. Cornejo IA, Ramalingam S, Fish JS, Reimanis IE. Hidden treasures: Turning food waste into glass. Am. Ceram. Soc. Bull. 2014 Aug 1;93:24-7.

23. Cornejo IA, Reimanis IE and Ramalingam S, Methods of making glass from organic waste food streams, US2015/ 0065329A1 (2015).

24. Bogeshwaran K, Kalaivani R, Ashraf S, Manikandan GN, Prabhu GE. Production of silica from rice husk. Int. J. ChemTech Res. 2014 Sep 30;6(9):4337-45.

25. Punj S, Singh K. Blue-green light emitting inherent luminescent glasses synthesized from agro-food wastes. Journal of Materials Science: Materials in Electronics. 2019 Feb 28;30:3871-81.

26. Kaur M and Singh K, Evolution of Ca_2SiO_4 and $Ca_3Si_2O_7$ crystalline phases synthesized from agro-food waste ashes. AIP Conf Proc 2093:020033 (2019).

27. Devi LL, Basavapoornima C, Venkatramu V, Babu P, Jayasankar CK. Synthesis of Ca_2SiO_4: Dy^{3+} phosphors from agricultural waste for solid-state lighting applications. Ceramics International. 2017 Dec 15;43(18):16622-7.

28. Devi LL, Jayasankar CK. Spectroscopic investigations on high-efficiency deep red-emitting Ca_2SiO_4: Eu^{3+} phosphors synthesized from agricultural waste. Ceramics International. 2018 Aug 15;44(12):14063-9.

29. Zhu C, Yang Y, Liang X, Yuan S, Chen G. Rare earth ions doped full-color luminescence glasses for white LED. Journal of luminescence. 2007 Oct 1;126(2):707-10.

30. Caldiño U, Bettinelli M, Ferrari M, Pasquini E, Pelli S, Speghini A, Righini GC. Rare earth doped glasses for displays and light generation. Advances in Science and Technology. 2014 Dec 11;90:174-8.

31. Kesavulu CR, Kim HJ, Lee SW, Kaewkhao J, Wantana N, Kothan S, Kaewjaeng S. Influence of Er^{3+} ion concentration on optical and photoluminescence properties of Er^{3+}-doped gadolinium-calcium silica borate glasses. Journal of Alloys and Compounds. 2016 Oct 25;683:590-8.

32. Niu L, Zhou Y, Zhu C, He Z, Meng X. Pr^{3+} doped oxyfluoride silicate glasses for LEDs. Ceramics International. 2019 Feb 15;45(3):4108-12.

33. Devi LL, Jayasankar CK. Novel reddish-orange color emitting Ca_2SiO_4: Sm^{3+} phosphors for white LED applications prepared by using agricultural waste. Journal of Luminescence. 2020 May 1;221:116996.

34. Niu L, Zhu C, Zhang M, He Z, Liu J, Xu Q, Wang Z. Eu and Dy doped borophosphosilicate glass-ceramics for near ultraviolet based light-emitting diode applications. Vacuum. 2019 Nov 1;169:108877.

35. Fernández-Rodríguez L, Balda R, Fernández J, Durán A, Pascual MJ. Structure and luminescent properties of Sm/Dy-doped $Sr_2MgSi_2O_7$ glass–ceramics. International Journal of Applied Glass Science. 2023 Jan;14(1):140-54.

36. Gao Y, Qiu J, Zhou D. Investigation of optical properties: Eu with Al codoping in aluminum silicate glasses and glass-ceramics. Journal of the American Ceramic Society. 2017 Jul;100(7):2901-13.

37. Li M, Zhou X, Zhang Y, Jiang F, Sha S, Xu S, Li S. Preparation and upconversion luminescent properties of Yb^{3+}/Er^{3+} doped transparent glass-ceramics containing CaF_2 nanocrystals. Ceramics International. 2020 Nov 1;46(16):25399-404.

38. Chhina MK, Singh K. Photoluminescence and structural properties of air-reduced rare-earth (Eu) doped calcium silicates derived using biomass wastes. Biofuels, Bioproducts and Biorefining. 2022 Mar;16(2):562-75.

39. Monisha M, Murari MS, Aloraini DA, Almuqrin AH, Sayyed MI, Naregundi K, Kamath SD. Sm^{3+} ions doped $Sm_2Si_2O_7$-based glass ceramics: Crystallization, luminescence and energy transfer process through heat treatment. Journal of Rare Earth. 2023 Aug 1;41(8):1144-52.

40. Alhodaib A, Ibrahim O, Abd El All S, Ezzeldin F. Effect of rare-earth ions on the optical and PL properties of novel borosilicate glass developed from agricultural waste. Materials. 2021 Sep 27;14(19):5607.

41. Truong NM, Sedano M, Durán A, Balda R, Pascual MJ, Klement R. Er/Yb co-doped $LiYF_4$ transparent oxyfluoride glass-ceramics with up-conversion optical properties. Ceramics International. 2023 Dec 15;49(24):41201-9.

42. Ravi Teja V, Sreenivasulu M, Chavan VK. Optical Applications of Europium ion doped Silicate Glasses: W-LED. Silicon. 2024 Mar 15:1-9.

43. Mirdda JN, Mukhopadhyay S, Sahu KR, Goswami MN. Enhancement of Optical and Electrical Properties of Pr^{3+} Doped $Na_2O–ZnO–TeO_2$ Glass Materials. Glass Physics and Chemistry. 2023 Oct;49(5):442-55.

44. Monisha M, Murari MS, Sayyed MI, Al-Ghamdi H, Almuqrin AH, Lakshminarayana G, Kamath SD. Thermal, structural, and optical behavior of Eu^{3+} ions in Zinc Alumino Boro-Silicate glasses for bright red emissions. Materials Chemistry and Physics. 2021 Sep 15;270:124787.

45. Liu W, Wang Y, Han X, Li L, Tang N, Wei Y, Zhang Q, Yu J, Xiao Z, Han L. Structure and luminescence of Pr^{3+}-doped oxyfluoride glass-ceramics containing $Na_5Y_9F_{32}$: Pr^{3+} nanocrystals. Journal of Luminescence. 2024 Mar 1;267:120404.

46. Maity A, Jana S. Excitation dependent tunable emission color of Eu^{3+}-Tb^{3+} co-doped titanium zinc sodium phosphate glass. Physics B: Condensed Matter. 2021 Oct 15;619:413186.

47. Mattu NK, Singh K. Structurally modified bioglasses synthesized using agro-food wastes and conventional sources for bone regeneration application. Ceramics International. 2023 Dec 1;49(23):38910-20.

48. Cullity BD, Smoluchowski R. Elements of X-ray Diffraction. Physics Today. 1957 Mar 1;10(3):50-

.

49. Yadav AK, Singh P. A review of the structures of oxide glasses by Raman spectroscopy. RSC advances. 2015;5(83):67583-609.

50. Redkov AV, Lipovskii AA, Tagantsev DK. Micro-Raman spectroscopy study of glass-ceramics with gradient of volume fraction of crystalline phase. Journal of the American Ceramic Society. 2016 Aug;99(8):2558-60.

51. Yuan K, Wang F, Gao J, Sun X, Deng Z, Wang H, Chen J. Effect of sintering time on the microstructure, flexural strength and translucency of lithium disilicate glass-ceramics. Journal of non-crystalline solids. 2013 Feb 15;362:7-13.

52. Raju MK, Rao RP, Vijayan N, Azeem PA. A novel orange-red Sm^{3+}-doped $CaSiO_3$ nanostructured phosphor derived from agro-food waste materials for white light applications. Ceramics International. 2021 Oct 1;47(19):26704-11.

53. Chhina MK, Singh K. Samarium doped calcium silicate derived from agro-food wastes and their structural, optical, and luminescent properties. Ceramics International. 2021 Aug 1;47(15):21588-98.

54. Handke M. Vibrational spectra, force constants, and Si-O bond character in calcium silicate crystal structure. Applied spectroscopy. 1986 Aug;40(6):871-7.

55. Chhina MK, Singh K. Dy^{3+} and inherent Ti^{4+} activated Ca_2SiO_4 near white light emitting phosphors synthesized from agro-food waste ashes. Ceramics International. 2020 May 1;46(7):9370-9.

56. Karan R, Pal P, Maiti PK, Das K. Structure, properties and in-vitro response of SiO_2-Na_2O-CaO-P_2O_5 system based glass-ceramics after partial replacement of Na_2O by Li_2O. Journal of Non-Crystalline Solids. 2021 Mar 15;556:120554.

57. Colomban P, Tournie A, Bellot-Gurlet L. Raman identification of glassy silicates used in ceramics, glass and jewellery: a tentative differentiation guide. Journal of Raman Spectroscopy: An International Journal for Original Work in all Aspects of Raman Spectroscopy, Including Higher Order Processes, and also Brillouin and Rayleigh Scattering. 2006 Aug;37(8):841-52.

58. Ma T, Wang X, Gao C, Liu X, Liang L, Wu C, Yan M. Effect of Dy_2O_3 intergranular addition on microstructure and magnetic properties of (Nd, Dy)–Fe–B sintered magnets. Materials Express. 2016 Feb 1;6(1):93-9.

59. McMasters OD, Gschneidner Jr KA, Bruzzone G, Palenzona A. Stoichiometry, crystal structures and some melting points of the lanthanide-gold alloys. Journal of the Less Common Metals. 1971 Oct 1;25(2):135-60.

60. Spedding FH, Beaudry BJ, Henderson DC, Moorman J. High-temperature enthalpies and related thermodynamic functions of the trifluorides of Sc, Ce, Sm, Eu, Gd, Tb, Dy, Er, Tm, and Yb. The Journal of Chemical Physics. 1974 Feb 15;60(4):1578-88.

61. Mondal K, Singh DK, Manam J. Spectroscopic behavior, thermal stability and temperature sensitivity of Ca_2SiO_4: Eu^{3+} red-emitting phosphor for solid-state lighting application. Journal of Alloys and Compounds. 2018 Sep 15;761:41-51.

62. Shrivastava R, Khaparde S. Luminescence studies of diopside doped with various concentrations of Dysprosium (III). Research on Chemical Intermediates. 2022 Mar;48(3):969-82.

63. Khan I, Rooh G, Rajaramakrishna R, Srisittipokakun N, Kim HJ, Kirdsiri K, Kaewkhao J. Luminescence characteristics of Sm^{3+}-doped lithium barium gadolinium silicate glasses for Orange LED's. Spectrochimica Acta Part A: Molecular and Biomolecular Spectroscopy. 2019 May 5; 214:14-20.

64. Rajesh D. Pr^{3+} doped new TZYN glasses and glass-ceramics containing $NaYF_4$ nanocrystals: Luminescence analysis for visible and NIR applications. Optical Materials. 2018 Dec 1;86:178-84.

65. Dang P, Li G, Yun X, Zhang Q, Liu D, Lian H, Shang M, Lin J. Thermally stable and highly efficient red-emitting Eu^{3+}-doped $Cs_3GdGe_3O_9$ phosphors for WLEDs: non-concentration quenching and negative thermal expansion. Light: Science & Applications. 2021 Feb 1;10(1):29.

66. Woo HJ, Chung SJ, Hill ML, Hadrick K, Kim T. Europium-Doped Calcium Silicate Nanoparticles as High-Quantum-Yield Red-Emitting Phosphors. ACS Applied Nano Materials. 2023 May 18;6(11):9884-91.

67. Jha K, Jayasimhadri M. Spectroscopic investigation on thermally stable Dy^{3+} doped zinc phosphate glasses for white light emitting diodes. Journal of Alloys and Compounds. 2016 Dec 15; 688:833-40.

68. Mahajan R, Kumar S, Prakash R, Kumar V, Choudhary RJ, Phase DM. X-ray photoemission and spectral investigations of Dy^{3+} activated magnesium pyrophosphate phosphors. Journal of Alloys and Compounds. 2019 Mar 10;777:562-71.

69. Lv H, Wang S, Su C, Zhang H, Guo Z, Wang L, Wang T, Wei Y. Preparation and luminescence properties of Dy^{3+}-doped transparent glass–ceramics containing $NaGd(WO_4)_2$. Journal of Materials Science: Materials in Electronics. 2020 May;31:6636-44.

70. McCamy CS. Correlated color temperature as an explicit function of chromaticity coordinates. Color Research & Application. 1992 Apr;17(2):142-4.

71. Mahajan R, Kumar S, Prakash R, Kumar V, Choudhary RJ, Phase DM. X-ray photoemission and spectral investigations of Dy^{3+} activated magnesium pyrophosphate phosphors. Journal of Alloys and Compounds. 2019 Mar 10;777:56